## Title

Development and Application of Preliminary TOGA Model for CO2-EOR with Comparison to Resistivity Data



## Author

Doughty, Christine

## Publication Date

2019-12-01

Peer reviewed

# Development and Application of Preliminary TOGA Model for $CO_2$-EOR with Comparison to Resistivity Data

Christine Doughty
Energy Geosciences Division
Lawrence Berkeley National Laboratory

December 2019

## Abstract

A new TOUGH code, TOGA (Transport of Oil, Gas, Aqueous), is used to model enhanced oil recovery (EOR) from a South Texas field where a combination of water, $CO_2$, and WAG (water-alternating-gas) injection wells are located in the down-dip region of a fault block, with oil and natural gas production occurring from wells located up-dip. The reservoir is composed of interlayered sands and shales at a depth of about 2000 m. TOGA considers three fluid phases (oil, gas, and aqueous), and multiple components. Oil field data including compositional analysis of stock-tank oil, gas-oil ratio, and gas gravity are used to determine the composition of oil and gas phases. Initial conditions for aqueous saturation are determined from a depth to surface resistivity survey conducted prior to the onset of $CO_2$ injection and Archie's Law. Simulation results after several years of EOR operations are then converted back to resistivity maps and compared to images created by time-lapse depth-to-surface resistivity surveys. These surveys show a strong increase in resistivity, interpreted as the replacement of aqueous phase by injected $CO_2$. In contrast, preliminary TOGA results show that injected $CO_2$ displaced more oil than water, suggesting that the three-phase relative permeability curves used to describe the interference of fluid phases need to be modified. Limited information on the composition of produced fluids provides another data set for comparison with model results. Model variations including using different relative permeability curve parameters and WAG cycle durations yielded improved model matches to the field data. The practical simplifications needed to simulate an actual operating oil field and the limited amount of field operation data available preclude using the present model to get an accurate history match or to make detailed predictions. Rather, the modeling is intended to illustrate the general trends occurring during $CO_2$-EOR and to indicate where more detailed information is needed.

## Introduction

The goal of this work is to apply advanced fluid flow modeling to gain understanding of the state of an oil reservoir where a series of depth to surface resistivity (DSR) surveys has been carried out during a $CO_2$-EOR operation by GroundMetrics, Inc., a small business that conducts electromagnetic geophysical surveys for petroleum resource exploitation. The fluid flow modeling is aimed specifically at calculating $CO_2$ storage as well as predicting the behavior of the reservoir fluids due to the ongoing injection/extraction process.

The work consists of three tasks: 1) Construction of a 3D reservoir-scale fluid-flow model of the oil field site, incorporating existing petrophysical, geological, and geophysical data, including resistivity models generated by GroundMetrics, from previous surveys of the field site area. 2) Running simulations with the fluid flow model to predict reservoir conditions over multiple periods of time, based on injection and production data provided by the field operator. 3) Assisting GroundMetrics in developing the connection between fluid flow, reservoir fluid saturations, and resistivity within the reservoir.

Because the multi-component flow and transport problem involves water, oil, natural gas, and $CO_2$ at reservoir conditions, a new numerical simulator, TOGA (Pan and Oldenburg, 2016), was used. TOGA is the only member of the TOUGH family of codes (Pruess, 2004) that can tackle this problem. TMVOC can handle similar fluid phases and compositions, but only for shallow systems (i.e., in and just below the vadose zone). EOS8 treats black oil and aqueous phases, but not $CO_2$ or natural gas. EOS7C considers $CO_2$ and $CH_4$, but not a separate oil phase. Given the importance of using $CO_2$ in EOR, both from economic and environmental perspectives, TOGA is a valuable addition to the TOUGH family of codes.

The work was conducted over a two-year period. In the first year the first two tasks were addressed using a rather coarse numerical model, as a proof of concept. In the second year, a number of model improvements were made, including development of a finer model grid, for use in all three tasks.

## Part 1: Year 1 activities

1.1 Model development
1.2 TOGA simulator
1.3 Simulations

## 1.1 Model development

### Model Geometry

The lateral extent of the numerical model is taken to be a closed fault block, denoted the BC Fault block, as shown in Figure 1.1, which illustrates the depth of the top of the Frio Formation, the formation into which water and $CO_2$ are injected and from which oil is produced. Figure 1.2 shows a zoomed-in view of just the BC fault block, illustrating the lateral limits of the model and the grid resolution. A coarse lateral grid resolution of 500 ft (152.4 m) was chosen for the preliminary model, with only 216 grid blocks per layer. A factor of three improvement in lateral resolution is planned for later generations of the model, to coincide with the 50 m resolution of the GroundMetrics surveys.

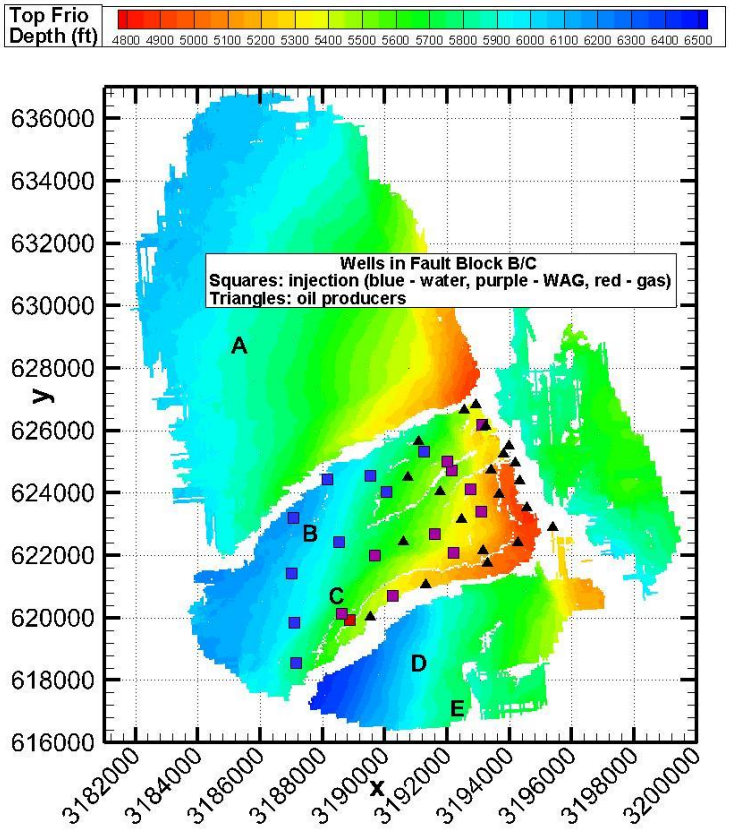


Figure 1.1. Top of Frio Formation, showing bottom-hole locations of wells in BC fault block. The x- and y-axes are in feet.

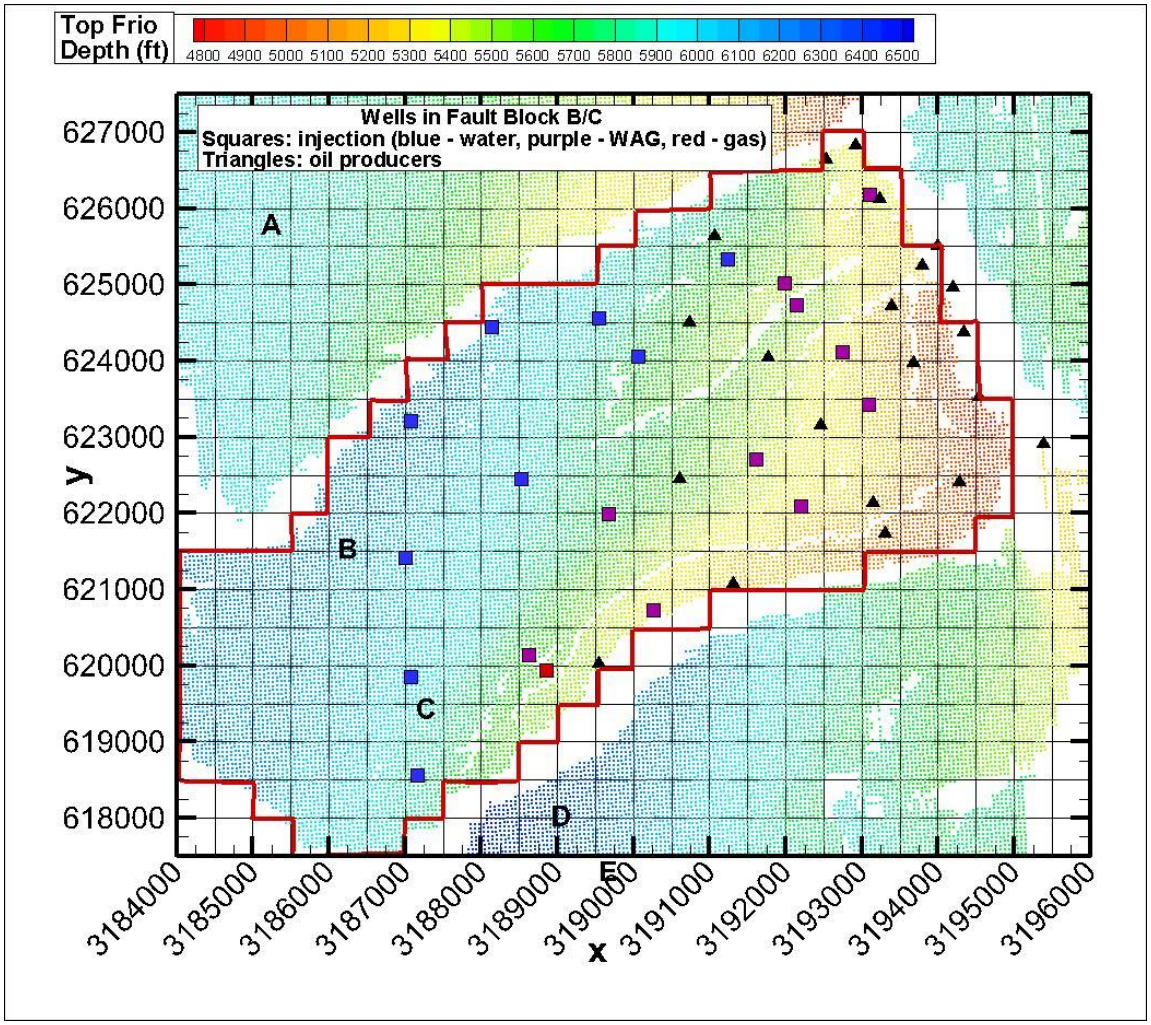


Figure 1.2. Lateral limits of the model (red line), grid resolution (black grid), and wells (symbols).

Vertically, the model represents the top six Frio A sands: A1, A2, A3, A4, A4L, and A5. Figure 1.3 shows the thickness for each sand, calculated by taking the difference between the top depth and base depth. The thicknesses were judged to be spatially uniform enough to warrant representing them as uniform-thickness layers in the model. Each sand is represented by one layer in the preliminary model, with horizontal permeability representing the sand permeability and vertical permeability representing the permeability of the inter-sand zones. Table 1.1 shows the thickness of each sand layer in the model. There are a total of 1296 grid blocks in the model. In later generations of the model, each sand may be subdivided into multiple model layers and the inter-sand zones may be discretized explicitly also. Moreover, the model layers need not be uniform, but could conform to actual thickness distributions shown in Figure 1.3.

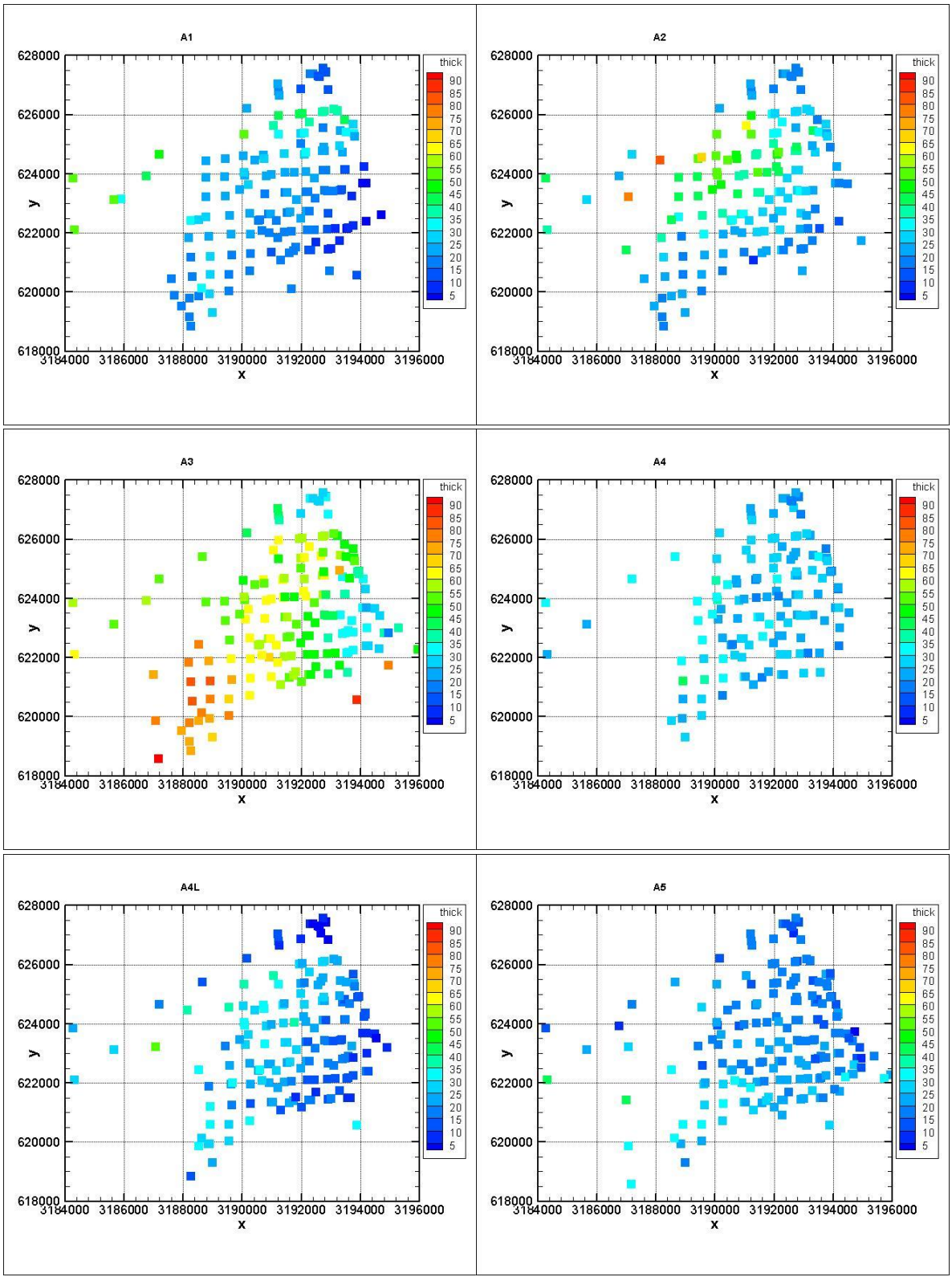


Figure 1.3. Thickness (in feet) of the six Frio A sands being represented in the model: A1, A2, A3, A4, A4L, and A5.

Table 1.1. Model thickness of Frio A sand layers.

| Sand | Range of Thicknesses Shown in Figure 1.3 (ft) | Thickness Used for Model (ft) |
|---|---|---|
| A1 | 20-25 | 23 |
| A2 | 35-40 | 39 |
| A3 | 55-60 | 59 |
| A4 | 25-30 | 29 |
| A4L | 20-25 | 23 |
| A5 | 20-25 | 23 |

Figure 1.4 shows the elevation of the top of the A1 sand, with elevation calculated by taking the difference of the Kelly Bushing (KB) elevation with respect to sea level and the measured depth. KB elevations do not vary appreciably over the BC fault block, so plots of depth and elevation are similar. The square symbols show the elevations at the well locations and the background contour map shows an interpolation of the well data onto a regular grid with the same resolution as the numerical model. Figure 1.5 shows the contour map, with purple lines drawn by hand to assess the possibility of representing the sands as stacked tilted planar structures. The orange and green lines were used to help calculate the slope of the plane: $9.43^{o}$ along the x (E-W) axis, $-4.61^{o}$ along the y (N-S) axis, and $10.09^{o}$ along the dip (direction of steepest descent). Insofar as the purple lines are parallel and equally spaced, a tilted plane is a reasonable representation. Figure 1.5 shows that over most of the BC fault block, a tilted plane is a good representation of the top of the A1 sand, although the local high at the northern corner of the fault block is not represented. In future generations of the model, the actual surface of the top of the A1 sand could be the top of the model.

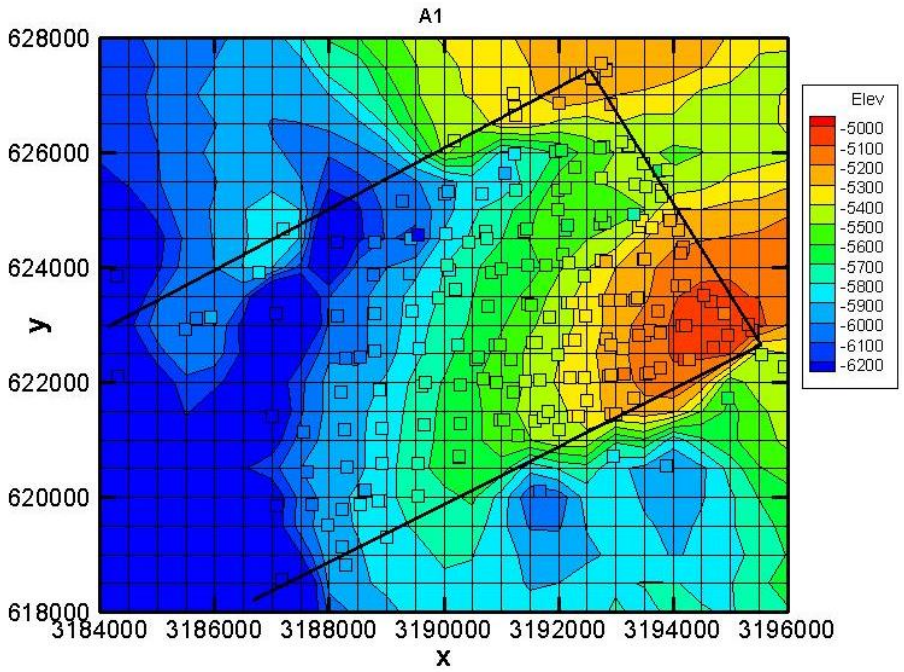


Figure 1.4. Contoured elevation (ft) of the top of the A1 sand: symbols show well data, heavy black line is the approximate lateral extent of the BC fault block.

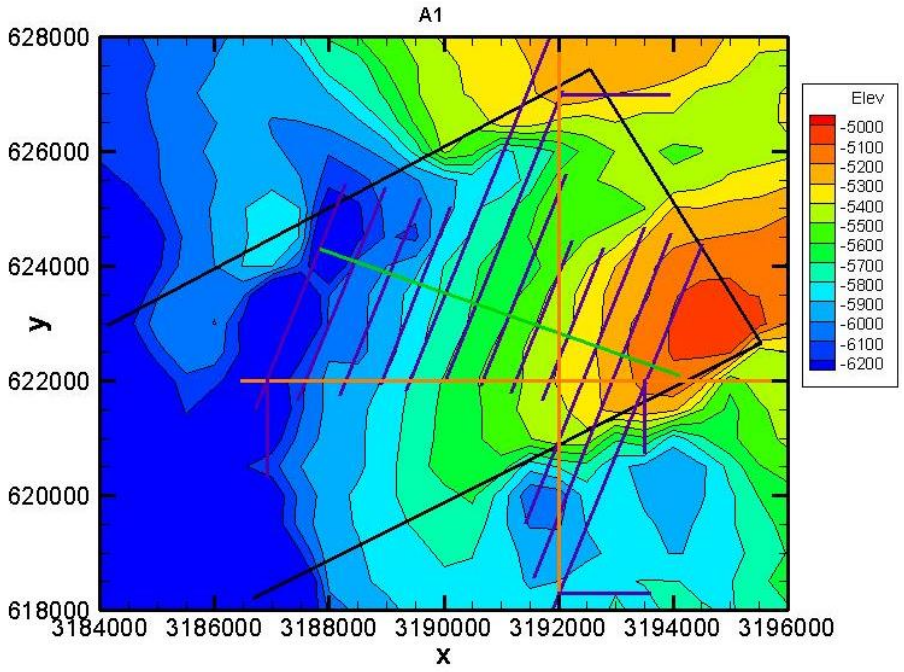


Figure 1.5. Contoured elevation (ft) of the top of the A1 sand with lines drawn by hand to assess the suitability of representing the sand by tilted planes (see text for description of details); heavy black line is the approximate lateral extent of the BC fault block.

### Initial and Boundary Conditions

The initial conditions for the model represent the state of the system prior to $CO_2$ injection. A resistivity distribution taken from well logs was interpolated onto a regular x,y,z grid, with x,y resolution equal to that of the numerical model (500 by 500 feet), and z resolution equal to half that of the original SEGY data set. With this construction, the (x,y) coordinates of the numerical model and the resistivity distribution are the same. The z origin of the numerical model can then be shifted up or down so that the entire model falls within the z range of the resistivity distribution. Then the shifted model coordinates of each grid block can be identified in the resistivity distribution and the resistivity can be converted to an aqueous saturation (the fraction of the pore space containing water) using Archie's Law, and assigned as an initial condition to that grid block. Archie's law is

$$S_a = (\rho_w/\rho)^{1/2}/\phi.$$

where $S_a$ is aqueous-phase saturation, $\rho_w$ is resistivity of water (0.035 ohm-m), $\rho$ is formation resistivity, and $\phi$ is formation porosity (0.3). Figure 1.6a shows the resistivity distribution in the top layer of the model (A1 sand) and Figure 1.6b shows the corresponding $S_a$ values.

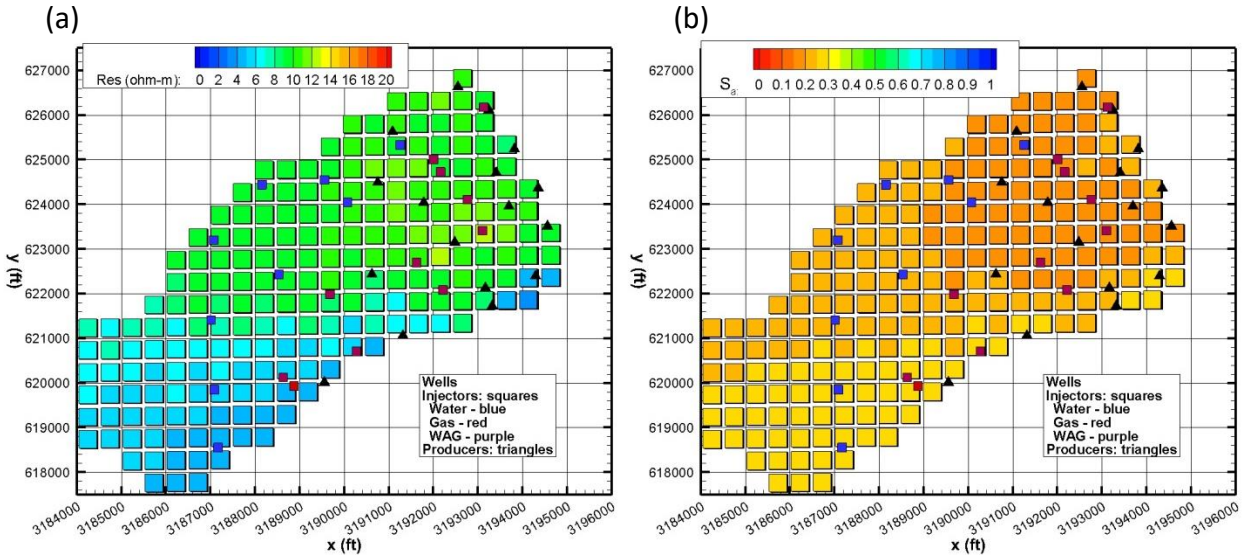


Figure 1.6. (a) Resistivity distribution in the top layer of the model interpolated from SEGY data; (b) $S_a$ distribution determined from resistivity distribution using Archie's law.

The initial pressure distribution is taken to be hydrostatic with a pressure of 2450 psi (169 bars) at 6234' (1900 m) depth, but the model will be allowed to equilibrate with gravity prior to simulating $CO_2$ injection, so this is just a convenient starting point. Initial temperature is taken to be a uniform 160°F (71°C), and temperature changes are not considered in the model (i.e., no energy equation is solved). In future generations of the model, a geothermal gradient can be applied as the initial condition (with the choice in the model of including temperature changes (solving energy equation) or not). If injected $CO_2$ or water temperature is much different from

reservoir temperature, then temperature changes may be significant and non-isothermal simulations can be done.

Gas gravity (0.65) is used to infer the composition of gaseous hydrocarbon (HC) components. Gas gravity is defined as the ratio of the molecular weight of the gas to the molecular weight of air (taken to be M = 28.8 g/mol). Assuming for simplicity that the gas is composed of methane (M = 16 g/mol) and ethane (M = 30 g/mol), simple algebra yields a mole fraction of 0.8 for methane and 0.2 for ethane in the gas phase (Table 1.2). The gas phase could be composed of methane plus a mixture of heavier hydrocarbons, and this may be explored in future generations of the model.

Mole fractions of liquid oil components are simplified from a compositional analysis study, with only constituents with a mole fraction of at least 0.02 included, similar components combined, and components heavier than decane combined into a pseudo-component. For the preliminary model, the same composition is assumed for all sands (a reasonable assumption), but components could be customized for each sand or even for each grid block if there were data to support this. Table 1.2 shows the mole fraction of oil components in the oil phase.

Table 1.2. Hydrocarbon components in the gas and oil phases for the model.

| **Component** | **Mole Fraction in the gas phase** |
|---|---|
| Methane | 0.80 |
| Ethane | 0.20 |
| **Component** | **Mole Fraction in the oil phase** |
| Hexane | 7.4 |
| Heptane | 9.3 |
| Octane | 7.4 |
| Nonane | 7.4 |
| Decane | 9.2 |
| Pseudo-component “C11-C18” | 59.3 |

.

All boundary conditions of the model are closed, that is, no-flow boundaries. If geologic information becomes available indicating that other boundary conditions (e.g., constant-pressure) would be more realistic, it will be straightforward to modify the model.

### Material Properties

The site operator reports 30-33% porosity, and 500-4000 md permeability. For the model, porosity is 0.3, sand permeability is 1000 md, and inter-sand layer permeability is 200 md. No field-relevant information on relative permeability and capillary pressure functions is available, so generic characteristic curves are taken from a $CO_2$-EOR sample problem in the TOGA User’s Guide. One feature of the relative permeability curves that is customized for the present problem

is residual aqueous phase saturation $S_{ar}$, which is generally the lower limit for $S_a$, and through Archie's Law, becomes the upper limit for resistivity. The original value of $S_{ar}$ was 0.2, which yields $\rho$ = 10 ohm-m, but this is decreased to 0.15 ($\rho$ = 17 ohm-m), consistent with field observations made in November 2015.

### Injection and Production Wells

Three types of injection wells are considered in the model (Figure 1.2): water, gas, and WAG (water alternating with gas). Injection wells are either perforated over the top three sands (A1, A2, A3) or the bottom three sands (A4, A4L, A5), in an alternating pattern moving updip. For the coarse model representation being used, it would not make sense to use a wellbore model. Instead, water injection is represented as a mass source in each of the three perforated layers in proportion to the thickness of the layer. Water wells are assumed to inject at a rate of 6000 BWPD, which converts to 10.8 kg/sec, assuming a water density of 982 kg/m$^3$ for injection conditions of 1850 psi (127 bar), 160$^o$F (71$^o$C). $CO_2$ injection rate is taken to be 15 MMSCFD, which converts to 9.1 kg/sec, assuming a $CO_2$ density of 1.85 kg/m$^3$ at STP. For WAG, a two-week water, two-week $CO_2$ schedule is assumed.

Production wells are assumed to be perforated over the entire sand sequence and to flow at a fixed bottom-hole pressure, $P_b$. In the absence of knowledge of the actual $P_b$ used in the field, a range of values will be used, and the simulated flow rate and composition will be compared to field data.

## 1.2 TOGA simulator

TOGA (**T**OUGH **O**il, **G**as, **A**queous; Pan and Oldenburg, 2016)) is a numerical reservoir simulator for modeling non-isothermal flow and transport of water, $CO_2$, multicomponent oil, and related gas components for applications including $CO_2$-enhanced oil recovery (CO2-EOR) and geologic carbon sequestration in depleted oil and gas reservoirs. It is a member of the TOUGH family of codes (Pruess, 2004) developed at Lawrence Berkeley National Laboratory, which are widely used for modeling a variety of problems, including geothermal reservoirs, oil and gas production, nuclear waste storage, environmental remediation, and $CO_2$ sequestration.

TOGA uses an approach based on the Peng-Robinson equation of state (PR-EOS) to calculate the thermophysical properties of the gas and oil phases including the gas/oil components dissolved in the aqueous phase, and uses a mixing model to estimate the thermophysical properties of the aqueous phase. The phase behavior (e.g., occurrence and disappearance of the three phases, gas + oil + aqueous) and the partitioning of non-aqueous components (e.g., $CO_2$, $CH_4$, and n-oil components) between coexisting phases are modeled based on the equal-fugacity principle that has been demonstrated to be very accurate as shown by comparison to measured data. Models for saturated (water) vapor pressure and water solubility (in the oil phase) are used

to calculate the partitioning of the water ($H_2O$) component between the gas and oil phases. All components (e.g., $CO_2$, $H_2O$, and n hydrocarbon components) are allowed to be present in all phases (aqueous, gaseous, and oil). TOGA uses a multiphase version of Darcy's Law to model flow and transport through porous media of mixtures with up to three phases over a range of pressures and temperatures appropriate to hydrocarbon recovery and geologic carbon sequestration systems. Transport of the gaseous and dissolved components is by advection and Fickian molecular diffusion.

Note that the present version of TOGA does not include salt, either dissolved in water or precipitated, so the salinity of the water, 100,000 ppm, cannot be represented in the model.

## 1.3 Simulations

### Check phase conditions

Initial conditions for TOGA are specified as pressure, temperature, $S_a$, and HC component mole fraction. The code then determines oil and gas phase conditions internally based on how HC components partition into gas, aqueous, and oil phases for the specified pressure and temperature. The code just needs to take one time step to accomplish this, so it runs very quickly. It turns out that using the HC mole fractions taken from Table 1.2 produces a reservoir with no gas phase, because all the $CH_4$ and $C_2H_6$ partitions into the oil phase.

For the Year 1 model, we erroneously assumed that the reported Gas Oil Ratio (GOR = 444 scf/bbl) represented reservoir conditions and therefore indicated that a gas phase should be present in the reservoir prior to $CO_2$ injection. Thus, the mole fractions of $CH_4$ and $C_2H_6$ were increased by trial and error until a gas phase formed. This error was corrected for the Year 2 model, and by comparing Year 1 and Year 2 model results, the effect of the extraneous gas phase was found to be minor.

### Establish stable initial conditions.

Next, the model is run with no sources and sinks for a long time, to do a pressure/gravity equilibration, in order to produce stable initial conditions for the subsequent history match simulations. For this simulation, the residual aqueous phase saturation $S_{ar}$ is increased to 0.3, greater than the values of $S_a$ (Figure 1.6b), so that the initial $S_a$ distribution (taken from the resistivity distribution) does not change. This simulation takes about 302 time steps to simulate 250 years, which requires about two hours. Figure 1.7 shows the initial and final pressure distributions. Note the decrease in P gradient from its initial value (hydrostatic) that arises from the oil-water-gas mixture in the reservoir being less dense than pure water. Figure 1.8 shows initial and final gas saturation distributions, illustrating the development of a gas cap. Figure 1.9 shows perspective views of the final pressure and gas and oil saturation distributions, to give a sense of the three-dimensional nature of the model.

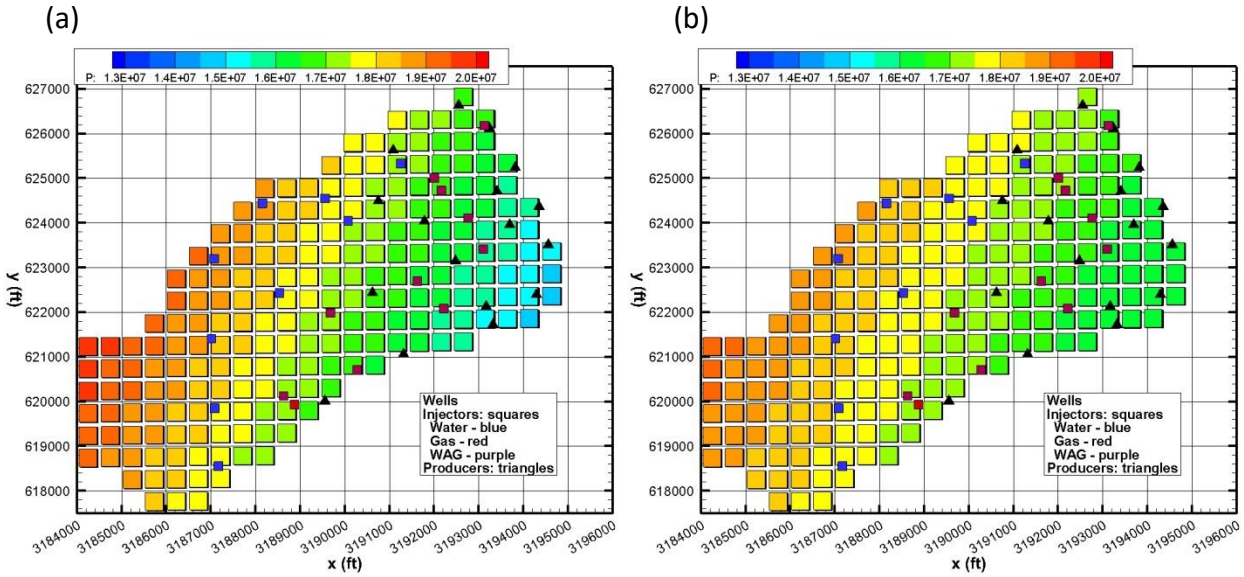


Figure 1.7. (a) initial and (b) final pressure distributions in the top layer of the model for the pressure/gravity equilibration simulation.

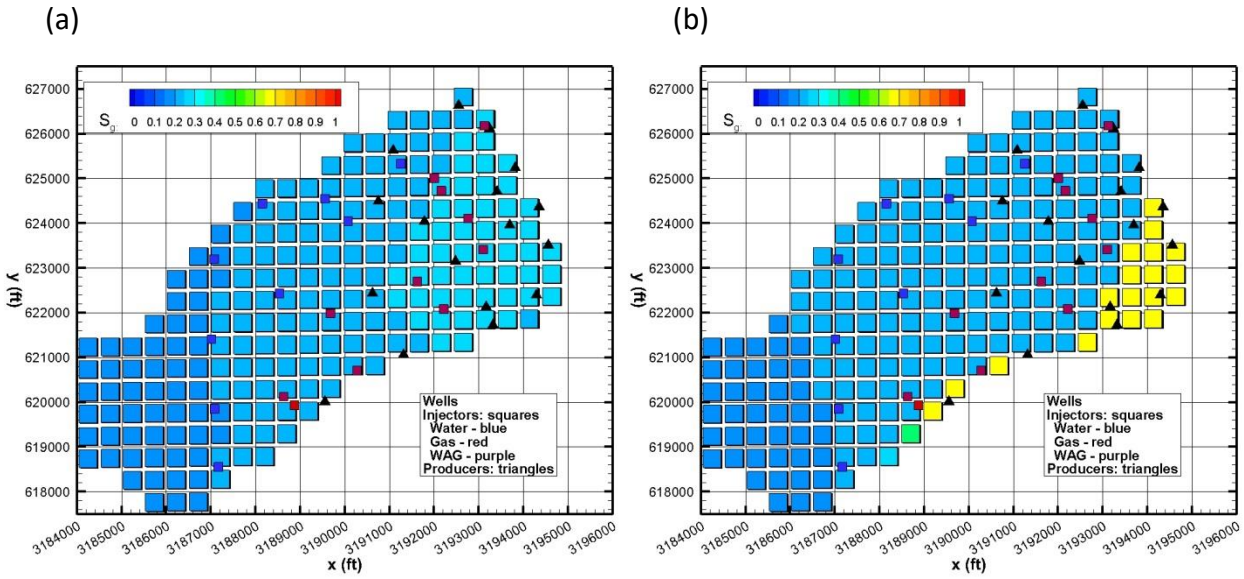


Figure 1.8. (a) initial and (b) final gas saturations distributions in the top layer of the model for the pressure/gravity equilibration simulation.

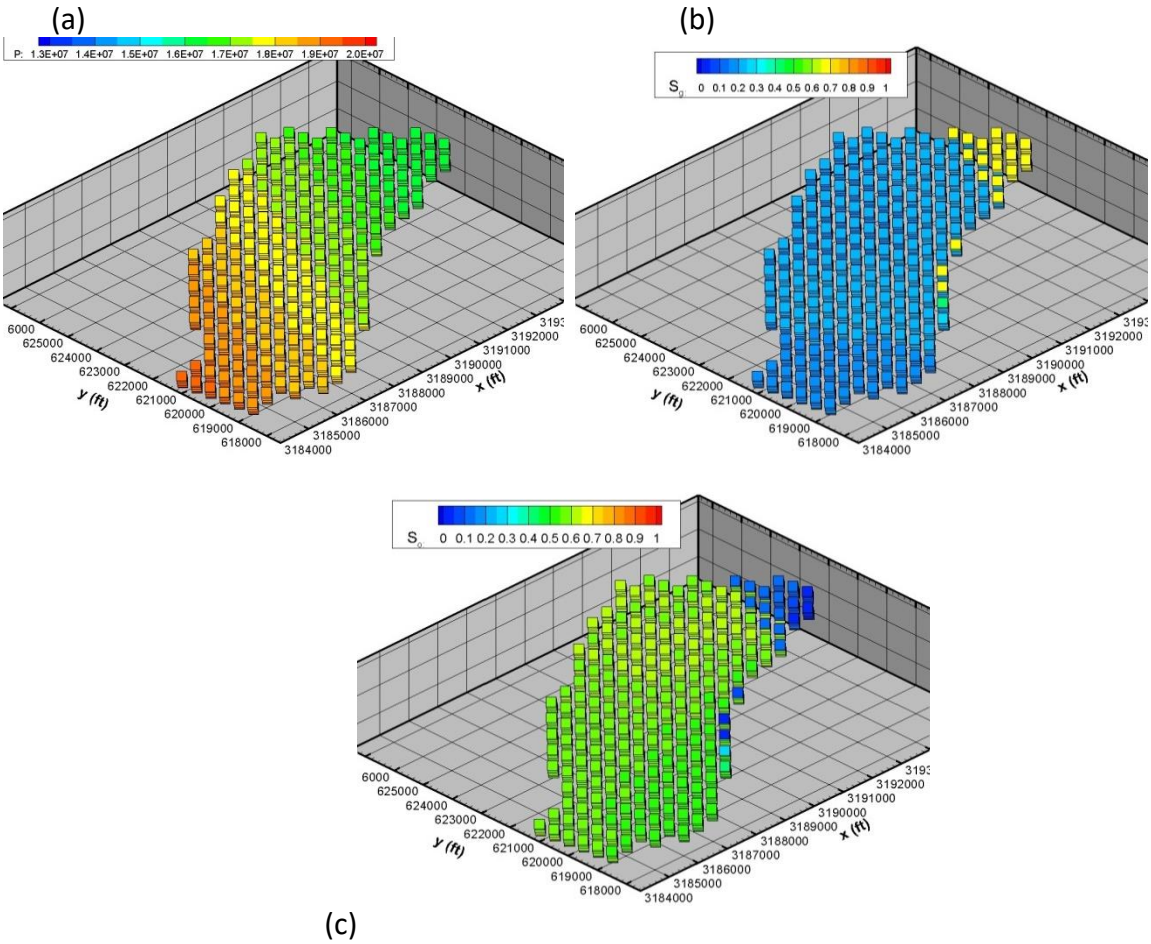


Figure1.9. Perspective views of (a) pressure distribution, (b) gas saturation distribution, and (c) oil saturation distribution at the end of the pressure/gravity equilibration.

## History Match

The history match simulation begins at t = 0, corresponding to November 5, 2014. For this simulation, oil production wells are held at a fixed pressure equal to 80% of the original reservoir pressure. This value is an estimate based on typical oil-field operations. Figure 1.10 shows P, $S_g$, $S_a$, and $S_o$ as a function of time for typical injection wells. The variation of pressure, gas saturation, and oil saturation are all expected, but the gradual increase of aqueous saturation for the WAG and gas-injection wells is surprising, and suggests that there may be overall fluid movement that is not localized around each injection well.

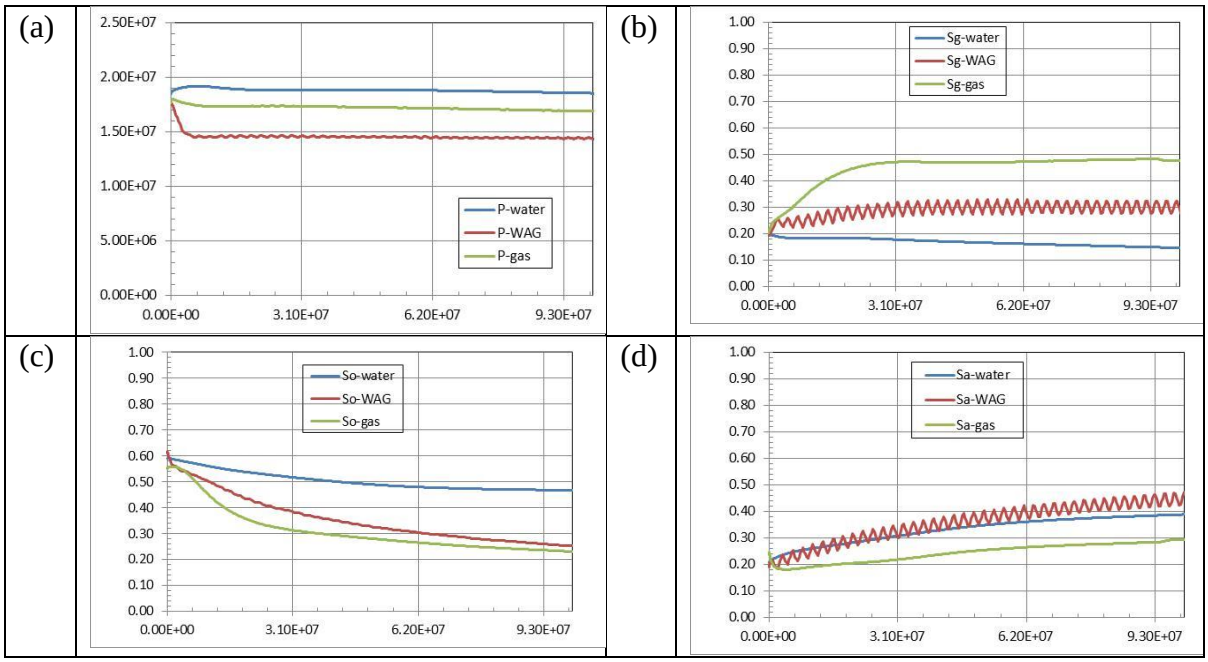


Figure 1.10. (a) Pressure (P), (b) gas saturation (Sg), (c) oil saturation (So), and (d) aqueous phase saturation (Sa) as a function of time at typical injection wells. Time is in seconds, so 3.1E7 corresponds to 1 year.

Figure 1.11 shows snapshots of key variables at 1 year (November 5, 2015), the time of the Groundmetrics survey, and Figure 1.12 shows the same snapshots at 3.25 years (February 5, 2018). One of the shortcomings of the simple way production is modeled (by holding the grid block containing the production well at constant pressure), is that the variables for those grid-blocks show the initial conditions rather than the current conditions in the reservoir.

The pressure distributions (P) show the expected effect of increased pressure near the injection wells (primarily down dip in the fault block) and decreased pressure near the production wells. Gas saturation ($S_g$) is generally increased in the up dip region. Recall that originally gas was primarily $CH_4$, but by one year the mole fraction of $CO_2$ in the gas phase (XCO2g) is significant and by 3.25 years it is dominant. Oil saturation ($S_o$) generally decreases in the up dip region. The resistivity shows a significant increase compared to the initial condition (Figure 1.6a), corresponding to a generally lower aqueous phase saturation ($S_a$).

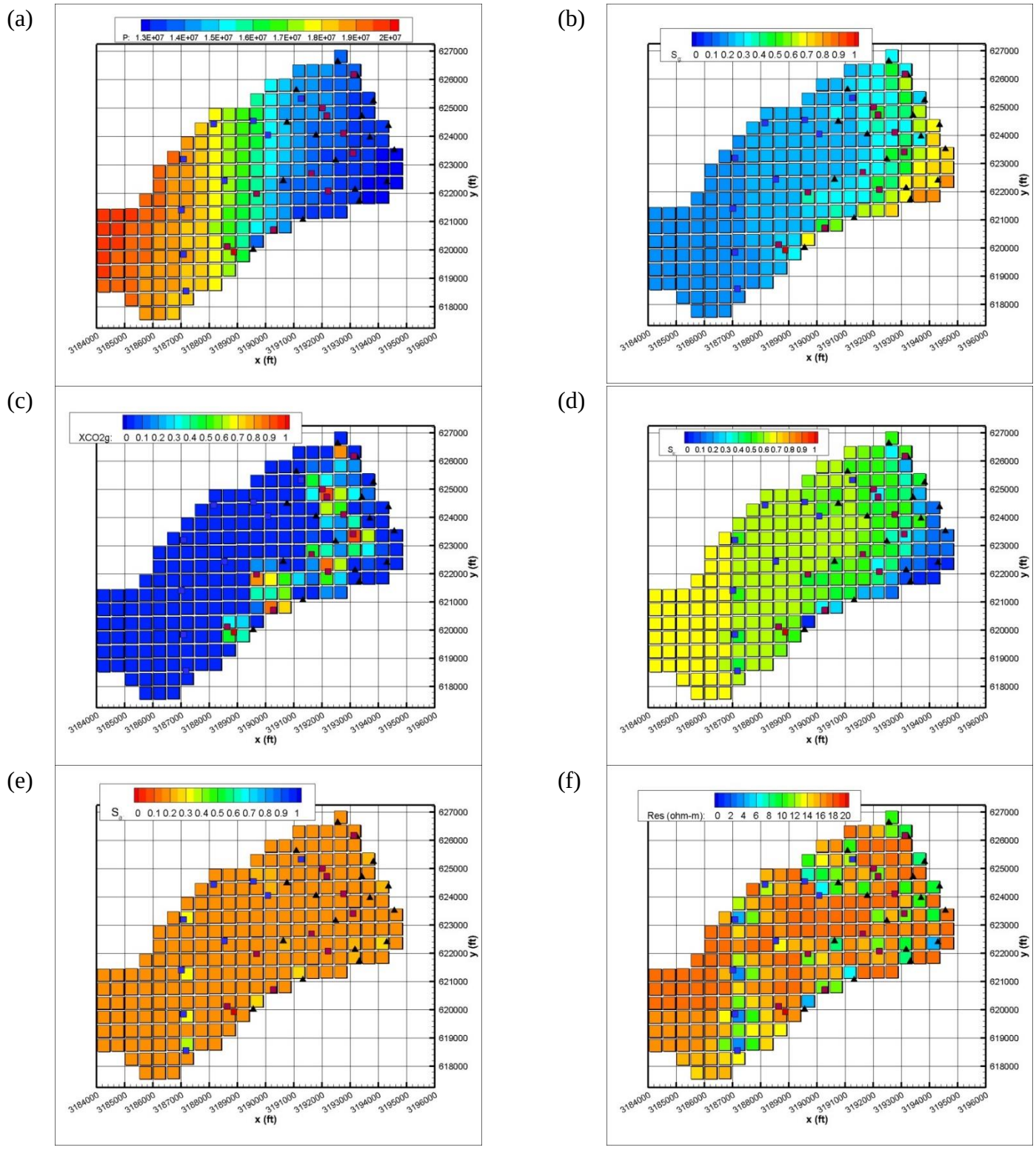


Figure 1.11. Simulation results for 1 year (November 5, 2015) for the top layer of the model. (a) Pressure P, (b) gas phase saturation $S_g$, (c) mole fraction of $CO_2$ in the gas phase (XCO2g), (d) oil saturation $S_o$, (e) aqueous phase saturation $S_a$. (f) resistivity.

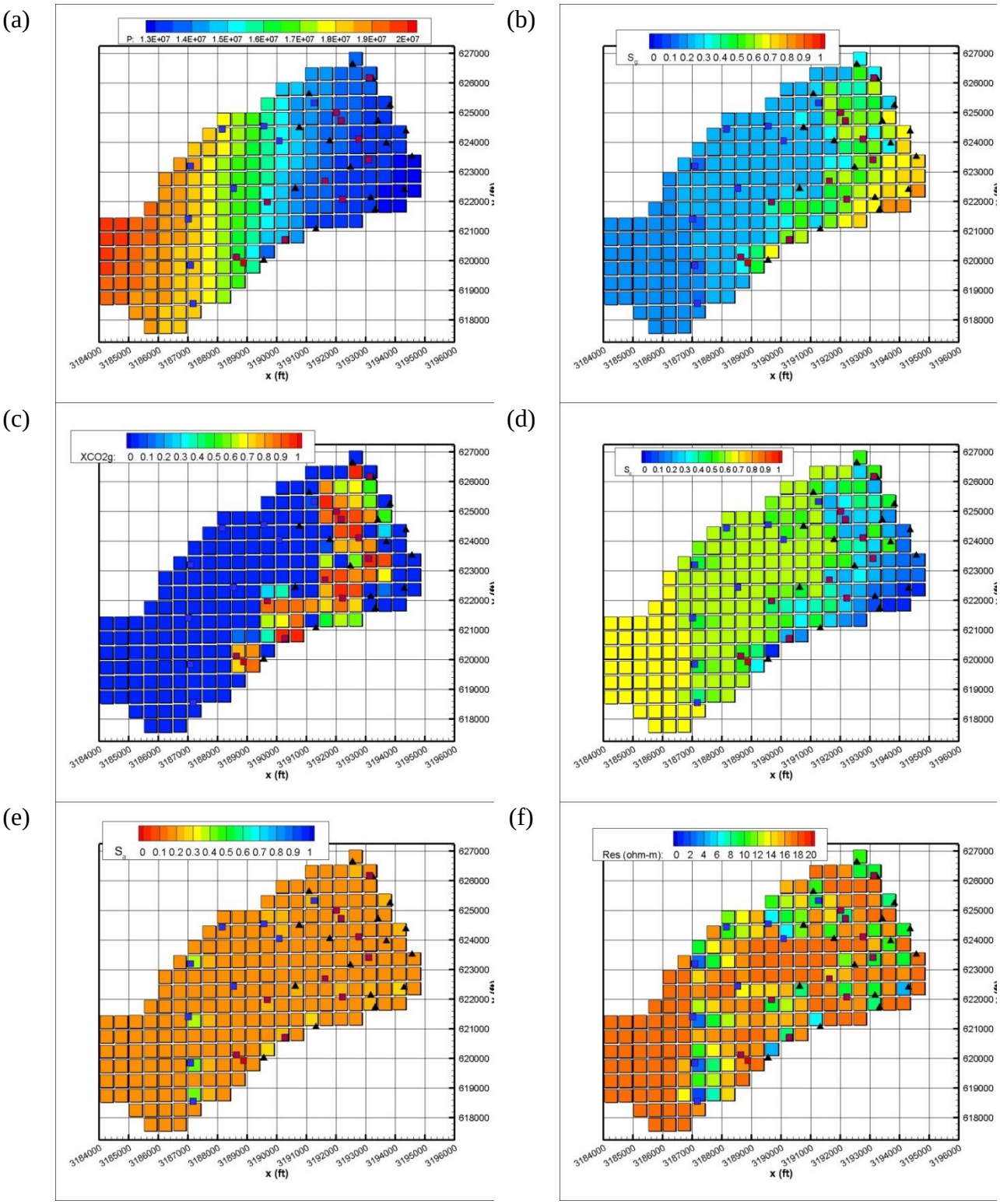


Figure 1.12. Simulation results for 3.25 year (February 5, 2018) for the top layer of the model. (a) Pressure P, (b) gas phase saturation $S_g$, (c) mole fraction of $CO_2$ in the gas phase (XCO2g), (d) oil saturation $S_o$, (e) aqueous phase saturation $S_a$. (f) resistivity.

# Part 2. Year 2 Activities

2.1 Improve model representation of production wells
2.2 Incorporate more operational information from field
2.3 Vary WAG schedule and residual saturation/compare model results to resistivity distribution
2.4 Correct model representation of initial reservoir conditions
2.5 Create consistent three-phase relative permeability curves
2.6 Design a finer grid
2.7 History match $CO_2$ injection
2.8 Conclusions

## 2.1 Improve model representation of production wells

In the initial version of the TOGA model, production was represented in a very simple way: by holding pressure constant in the grid elements representing production wells, and monitoring the amount of fluid that flowed into that well. For the coarse lateral grid resolution employed (150 m), this method has two disadvantages. First, it does not account for near-well pressure gradients, and second, it makes display of spatial distributions of pressure and phase saturation problematic because production wells show up as constant-property zones, rather than showing the actual values. The latter problem has been resolved by creating extra elements at the location of production wells that are connected to the main grid by one connection. These extra elements are then held at constant pressure. When the grid resolution is improved (Section 6 below), the former problem will also be ameliorated, but an even better solution would be to use TOUGH's deliverability option for all production wells. This was attempted unsuccessfully in the initial version of the model, because a few locations where injection wells and production wells were very close to one another caused numerical problems and the code ran very slowly. If the deliverability option can run efficiently, it is the most realistic way to model production.

## 2.2 Incorporate more operational information from field

The site operator provided detailed well logs showing flow and tracer test results that identified flowing intervals in 18 wells: 3 production wells, 14 injection wells, and one well that does not appear in the files with well locations and formation tops. Of the 17 remaining wells, 12 are already in the model: 5 water injection wells, 1 WAG injection well, and 6 production wells. The other 5 wells are identified as WAG injection wells, but previously were identified as monitoring wells, so were not explicitly represented in the model. Figure 2.1 shows a plan view of the model with the wells with new information shown with open symbols.

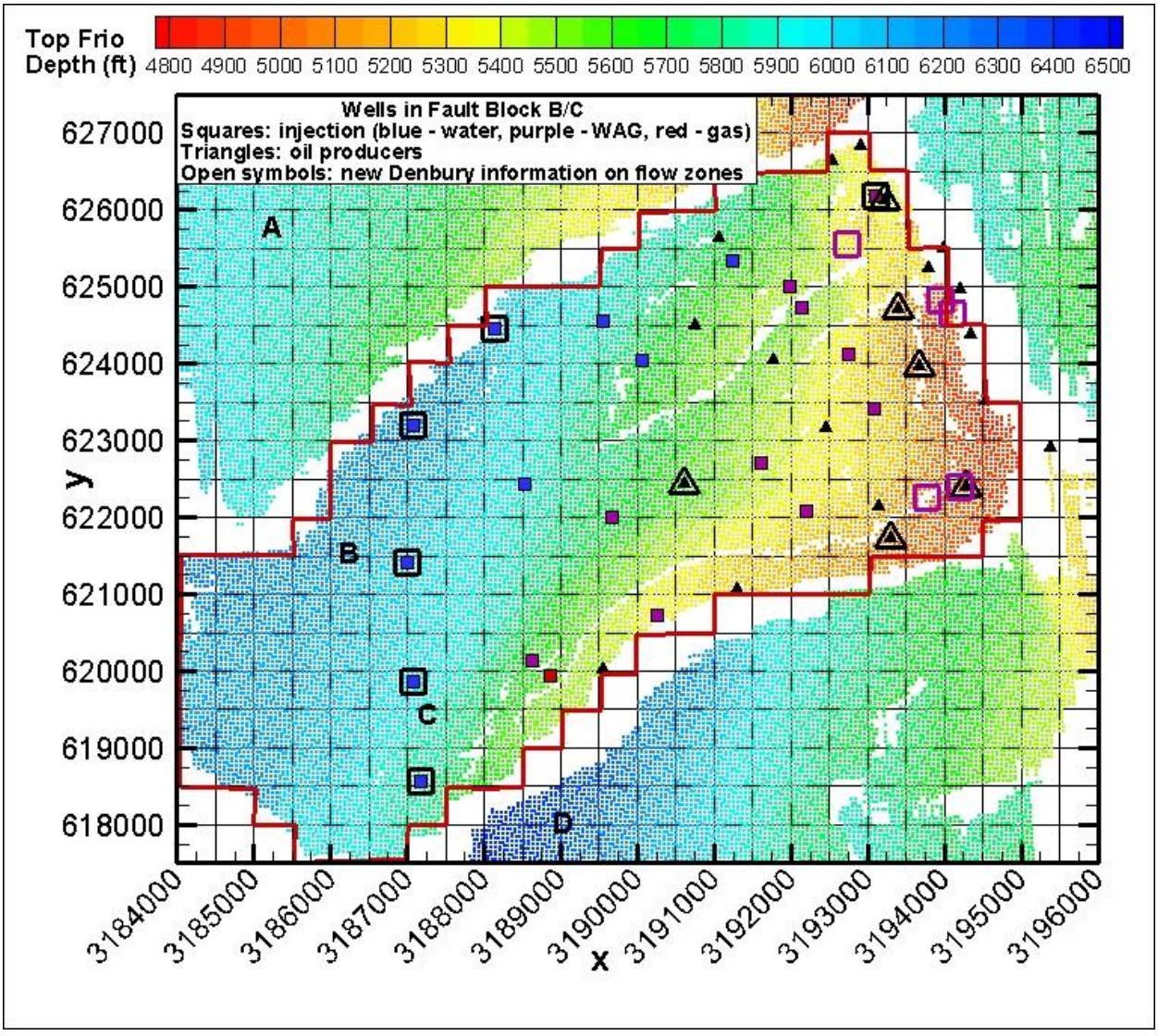


Figure 2.1. Plan view of model with wells having new information identified by open symbols.

## 2.3 Vary WAG schedule and residual saturation/compare model results to resistivity distribution

Figure 2.2 (Left) shows the resistivity distribution in the top sand layer after one year of $CO_2$ injection, determined from GroundMetrics Depth to Surface Resistivity (DSR) survey. Figure 2.2 (Right) shows the corresponding aqueous phase saturation distribution from Archie's Law.

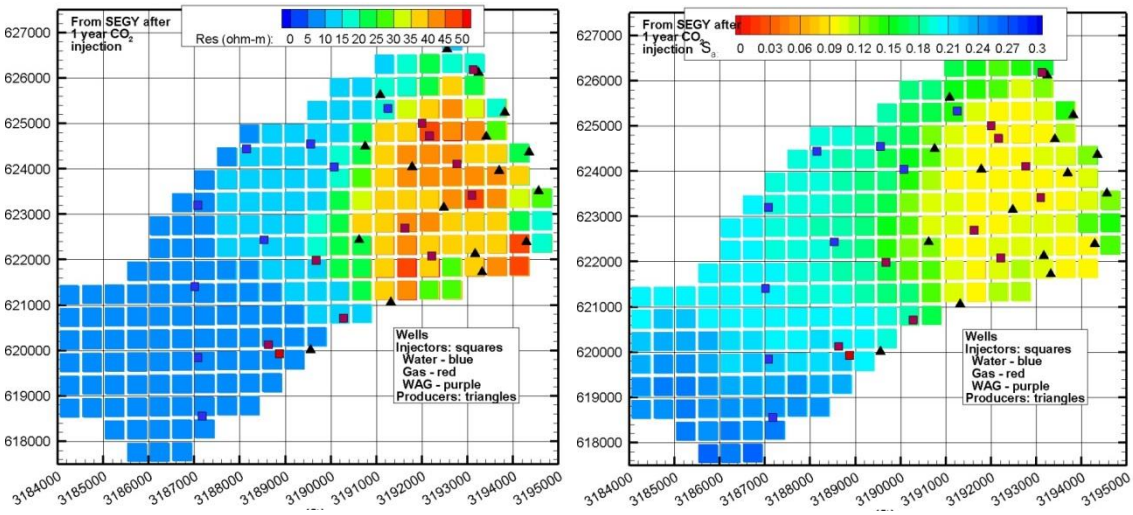


Figure 2.2. (Left) Field data for resistivity, plotted at the resolution of the model grid, in the top sand layer after one year of $CO_2$ injection. (Right) The corresponding aqueous saturation distribution, determined from the resistivity distribution using Archie's Law.

Figure 2.3 shows TOGA model results converted to resistivity from aqueous phase saturation using Archie's law in the top sand layer before (left) and after (right) one year of $CO_2$ injection, using two-week WAG cycles (i.e., two weeks of water injection and two weeks of $CO_2$ injection). Note that there is hardly any increase in resistivity, and the model results do not compare well to the field data.

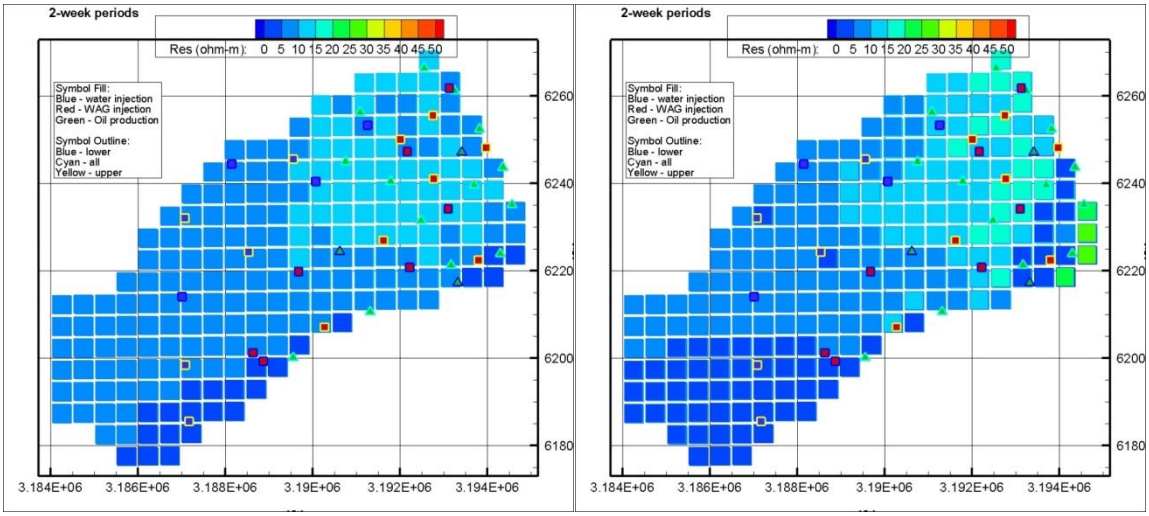


Figure 2.3. Modeled resistivity distributions in the top sand layer, before (Left) and after (Right) one year of $CO_2$ injection.

To try to find a better match between model and observation, three different WAG schedules were modeled: 4-month cycles, 6-month cycles, and 1-year cycles. Figure 2.4 shows the model results after one year (for the 1-year cycle, WAG wells inject $CO_2$ for the entire year).

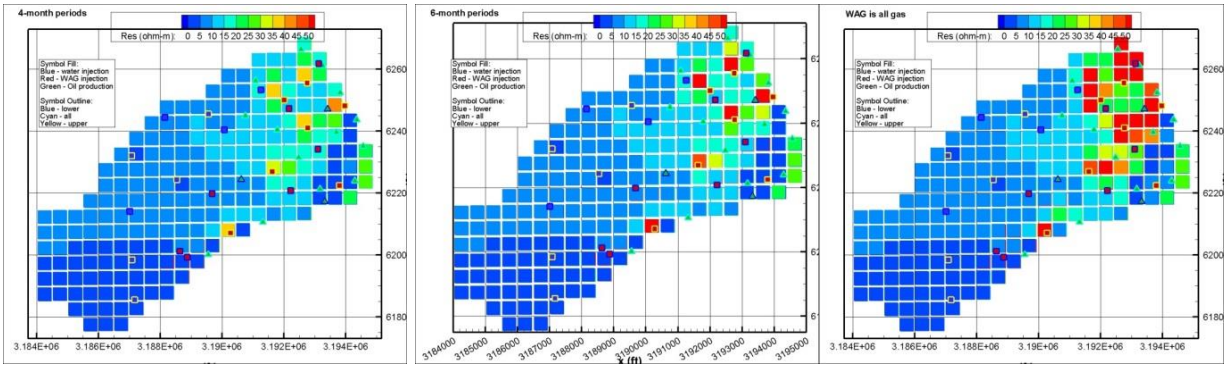


Figure 2.4. (Left) 4-month WAG cycle, (Middle) 6-month WAG cycle, (Right) 1-year WAG cycle; modeled resistivity distributions in top sand layer.

The longer the WAG cycle, the bigger the resistivity. All the model results show more localized high-resistivity regions than the field data shows, but it is clear that longer WAG cycles produce a resistivity distribution that is more like the field data.

Figure 2.5 shows modeled aqueous phase saturation distributions after one year of $CO_2$ injection for two different values of residual saturation for the aqueous phase, $S_{wr}$, which determines how much water remains trapped in the formation as $CO_2$ or oil flows by. In the left frame, $S_{wr}$ = 0.05 and in the right frame, $S_{wr}$ = 0.10. Compared to the field data, the aqueous phase saturation near the WAG injection wells is a little too small for $S_{wr}$ = 0.05 and a little too big for $S_{wr}$ = 0.10, suggesting that an intermediate value is appropriate.

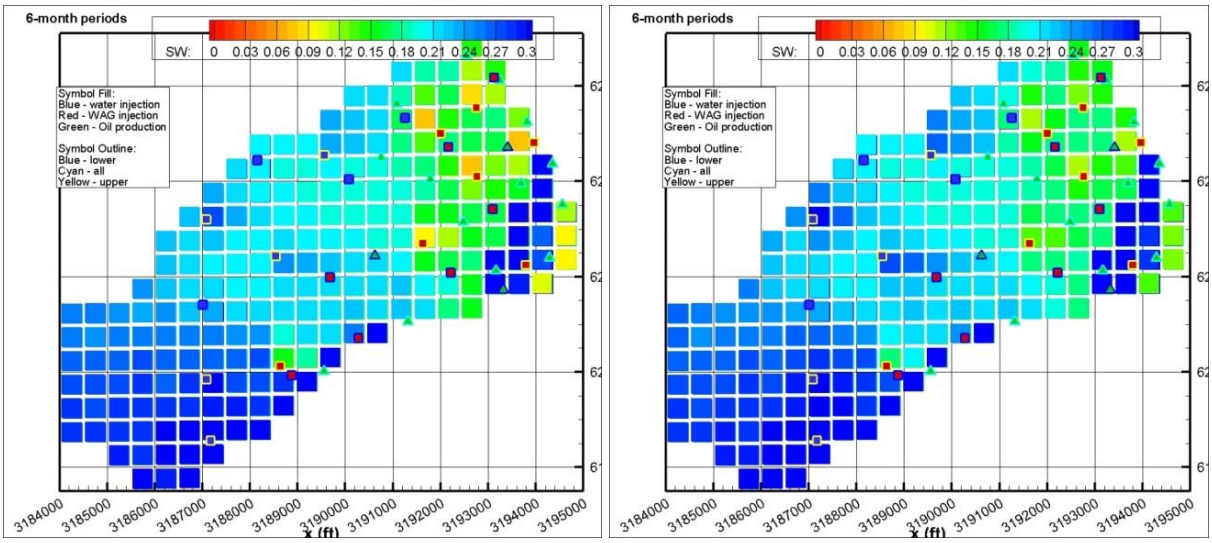


Figure 2.5. Modeled aqueous phase saturation distribution in top sand layer after one year $CO_2$ injection. (Left) residual aqueous phase saturation 0.05, (Right) residual aqueous phase saturation 0.10.

## 2.4 Correct model representation of initial reservoir phase conditions

As in Year 1, Archie's Law is used to convert the field resistivity distribution to an aqueous phase distribution for the model initial condition, gas gravity determines the composition of the gas phase, and mole fractions of liquid oil components are simplified from a compositional analysis study. TOGA then takes one step to determine oil and gas phase conditions internally based on how HC components partition into gas, aqueous, and oil phases for the specified pressure and temperature. This produces initial reservoir conditions with no gas phase – all $CH_4$ and $C_2H_6$ is dissolved. In contrast to Year 1, where gas components were arbitrarily increased until a gas phase formed, for Year 2 the initial conditions do not include a gas phase, which is believed to better represent actual reservoir conditions prior to $CO_2$ injection.

## 2.5 Create consistent three-phase relative permeability curves

In preliminary sensitivity studies of relative permeability curves (Section 3 above), residual saturation of the aqueous phase $S_{wr}$ was varied without altering anything else in the relative permeability curves. However, for three-phase relative permeability curves, a more careful approach is required to create internally consistent relative permeability curves, as parameters such as residual saturation impact the curves in multiple ways. The three-phase relative permeability curves being used in TOGA were programmed into an Excel spreadsheet, so the impact of varying individual parameters on all curves could be assessed, and a set of parameters that produces the best match to the field data, denoted "Average 1&2, more mobile gas" was chosen. The top two frames of Figure 2.6 show water (aqueous) and gas relative permeability for several different sets of parameters. Relative permeability to water and gas just depends on water saturation $S_w$ and gas saturation $S_g$, respectively. The lower frame shows oil relative permeability as a function of oil saturation $S_o$ for a range of $S_g$, using the parameters of the curves labeled "Average 1&2, more mobile gas". Relative permeability to oil depends on all phase saturations, but since $S_w + S_g + S_o = 1$, only two saturations need be specified.

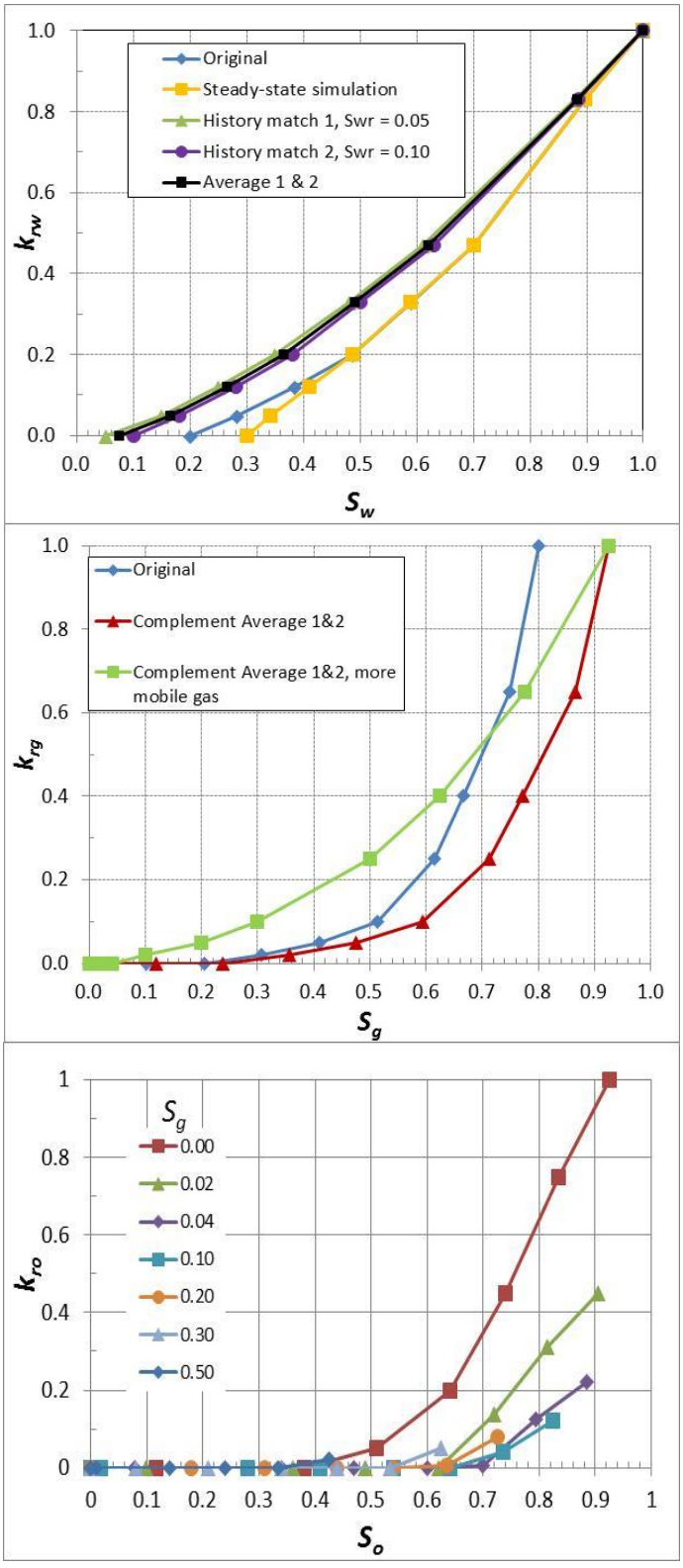


Figure 2.6. Three-phase relative permeability curves for various model parameters (top two frames) and for chosen parameters (bottom frame).

## 2.6 Design a finer grid

The original grid had cells with lateral size 150 m by 150 m. The new finer grid subdivides each cell into 9 smaller cells, each 50 m by 50 m. Figure 2.7 shows the new grid. The red line shows the lateral boundary of the model, which is closed on all sides. Vertical discretization is unchanged from the original grid, with six layers, each representing one sand layer.

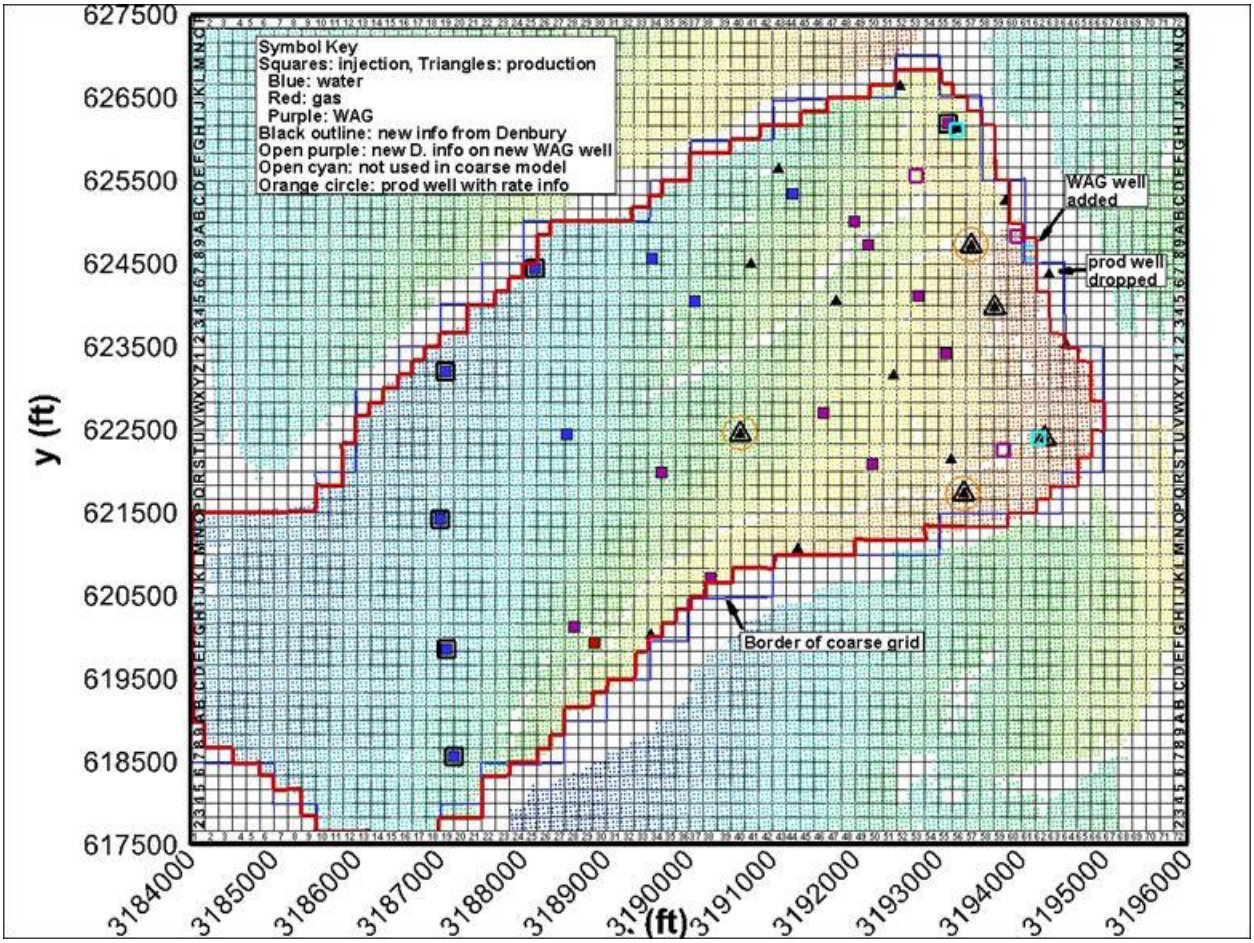


Figure 2.7. Refined grid showing wells with new information from site operator.

## 2.7 History match $CO_2$ injection

The history-match simulation begins at t = 0, corresponding to November 5, 2014. Figure 2.8 shows the field resistivity distribution, plotted at the resolution of the finer grid, prior to $CO_2$ injection, and the corresponding aqueous phase saturation distribution, calculated with Archie's Law, which provides the initial conditions for the history-match simulation. Figure 2.9 shows the field resistivity distributions inferred from the DSR survey conducted one year later, and the corresponding aqueous phase saturation distributions, which are the results the model will be compared to. Note that each injection well is labeled either U for upper or L for lower, indicating into which sand layers injection occurs: Sands 1, 2, 3 for upper, and Sands 4, 4L, and 5 for lower. Most injection wells are screened over all six sand layers, because we do not have specific information on the actual open intervals, but for three production wells, we know they are open in the lower sands – these are labeled L in Figures 2.8 and 2.9. It is interesting to compare Figures 2.2 and 2.9, which show the one-year field resistivity distributions plotted on coarse and fine grids, respectively. Using a finer grid enables near well variability to be seen, especially in Frio Sand 4.

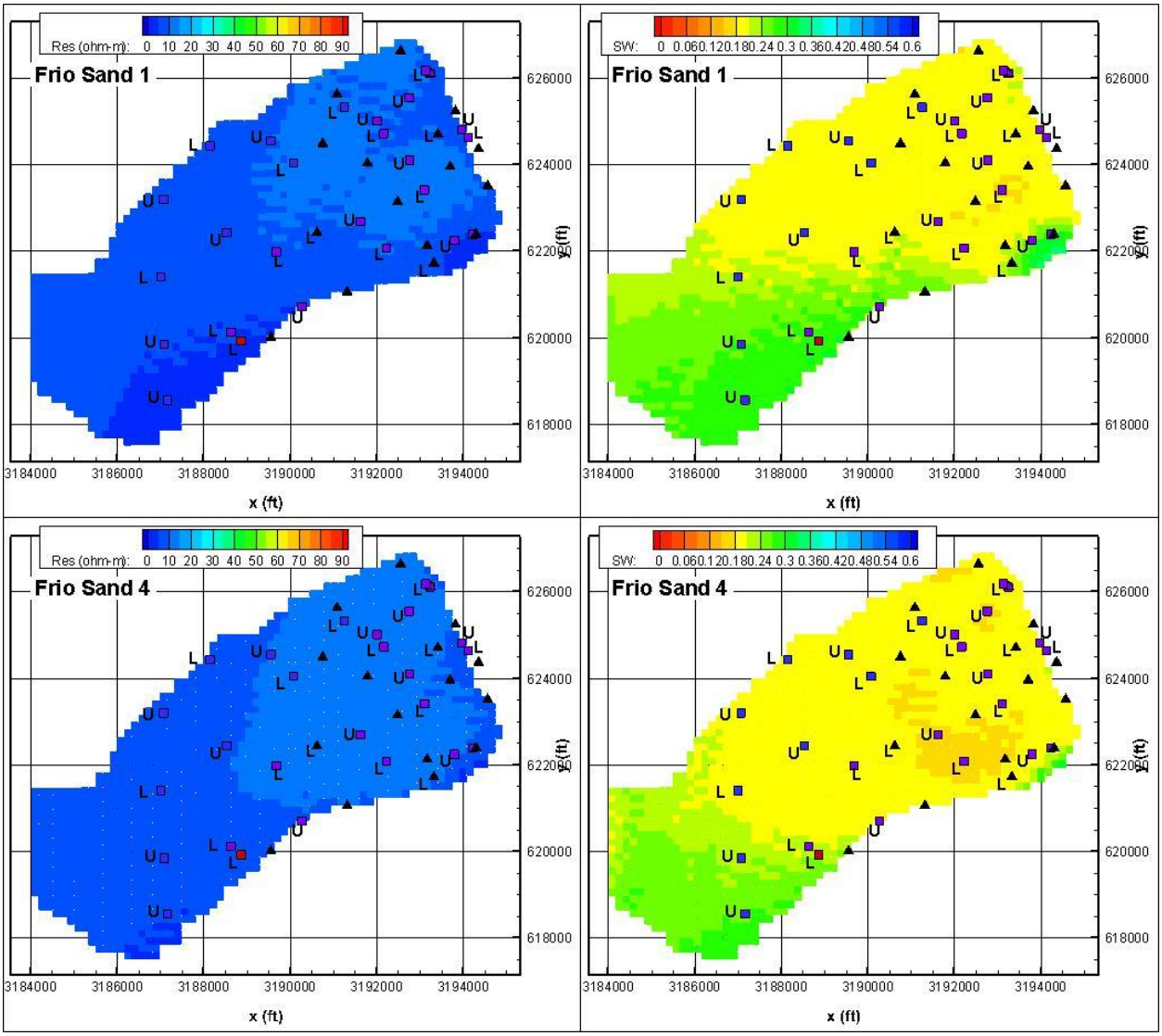


Figure 2.8. (Left) Field resistivity data prior to $CO_2$ injection, plotted at the resolution of the finer model grid, and (Right) corresponding aqueous phase saturation distribution from Archie's Law, for Frio Sand 1 and Frio Sand 4

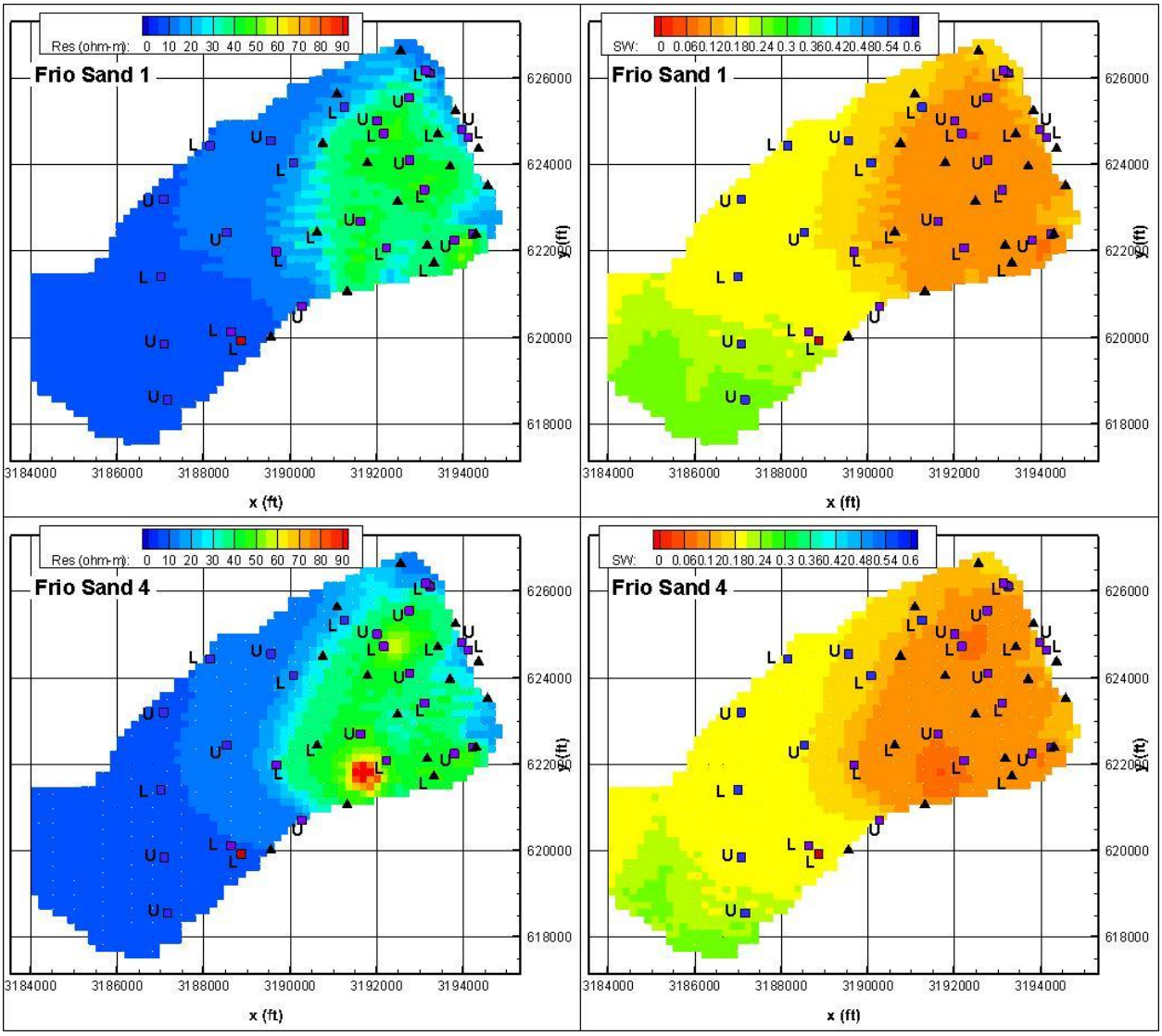


Figure 2.9. (Left) Field resistivity data after one year $CO_2$ injection, plotted at the resolution of the finer model grid, and (Right) the corresponding aqueous phase saturation from Archie's Law.

For the history-match simulations, oil production wells are held at a fixed pressure equal to 60% of the original reservoir pressure. While lower than the pressure used for the Year 1 studies, this value is within the range of typical oil-field operations. Numerical studies have shown that TOGA sometimes runs better when bigger pressure perturbations are imposed, and the lower fixed pressure was chosen for computational expediency. Based on the previous sensitivity studies, in which the better matches to the field data were produced for longer WAG cycles, here we consider a constant injection rate (equivalent to a 1-year WAG period). Figure 2.10 shows one-year results for the original production rate and Figure 2.11 shows one-year results for half that rate, which could be considered as a time-averaged representation of a 6-month WAG period. Figure 2.12 shows the half-rate case after two years of operation. Results for two of the

six model layers are shown, Frio Sand 1 and Frio Sand 4. Results for Frio Sands 2 and 3 are similar to those for Frio Sand 1, and results for Frio sands 4L and 5 are similar to those for Frio Sand 4.

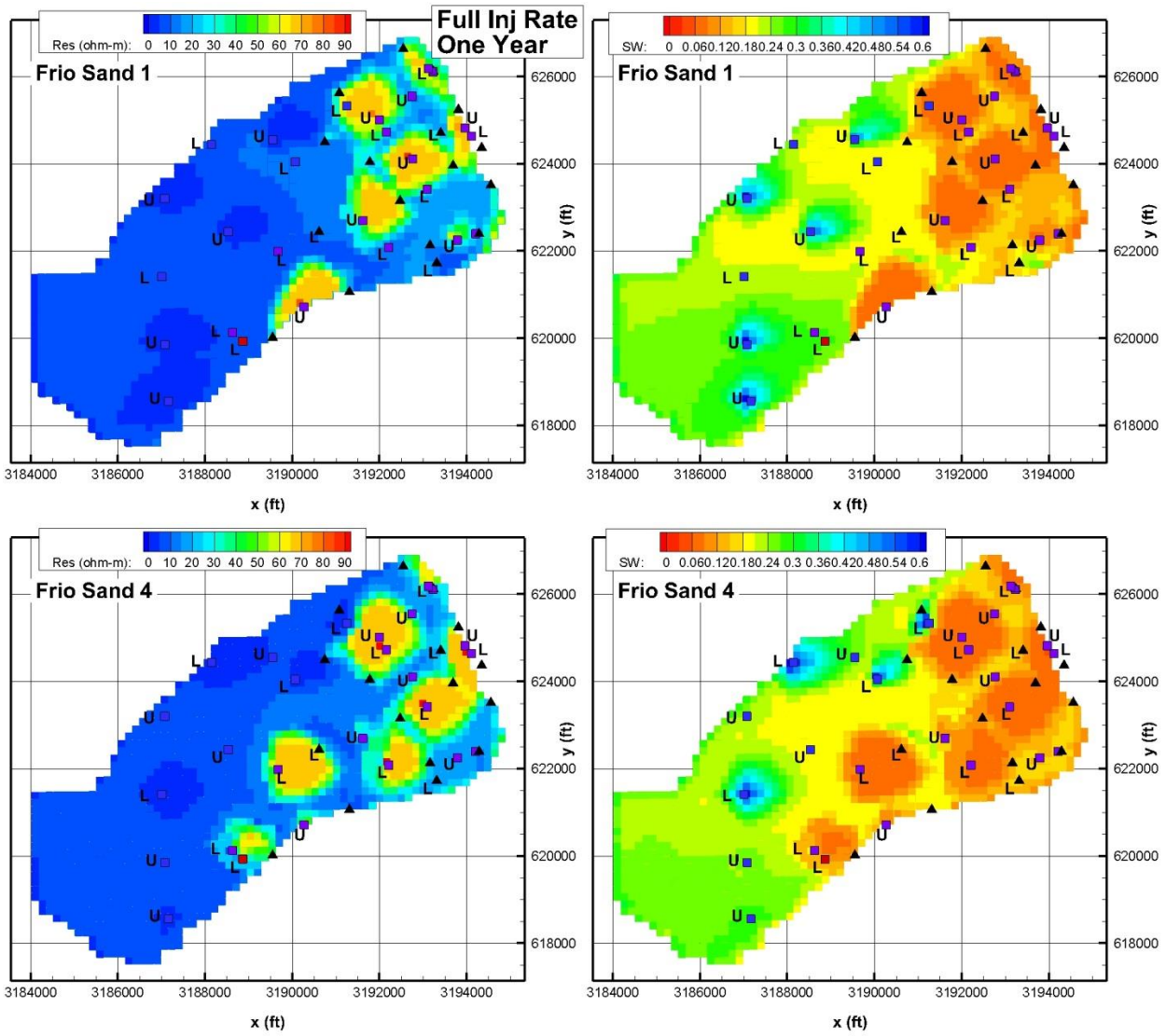


Figure 2.10. Model results for one year of $CO_2$ injection at the full injection rate, for the top model layer (Frio Sand 1) and the fourth model layer (Frio Sand 4). The basic result is the aqueous phase saturation distribution, shown on the right, with resistivity, shown on the left, obtained from Archie's Law.

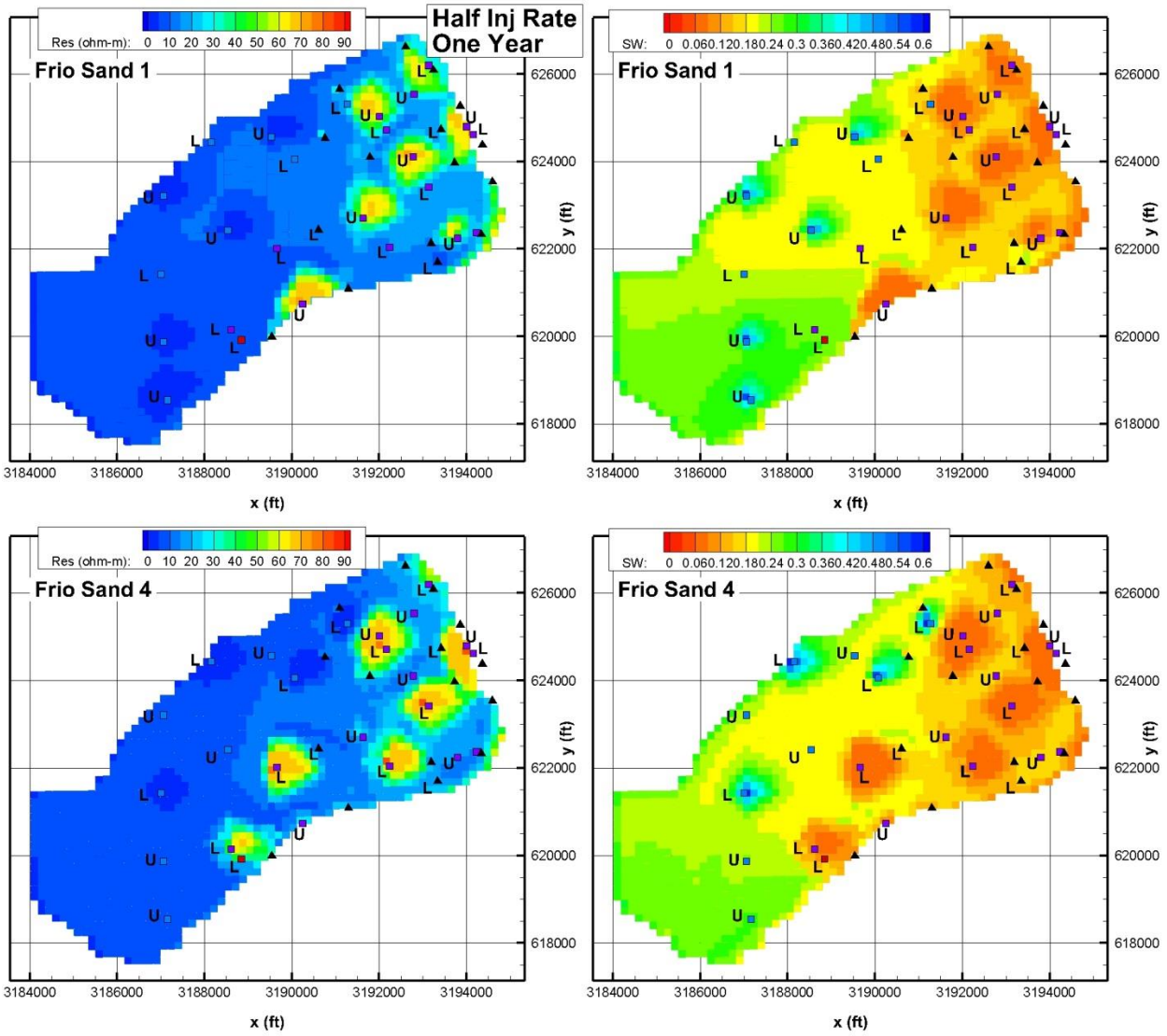


Figure 2.11. Model results for one year of $CO_2$ injection at half the injection rate, for the top model layer (Frio Sand 1) and the fourth model layer (Frio Sand 4). (Left) resistivity, (Right) aqueous phase saturation).

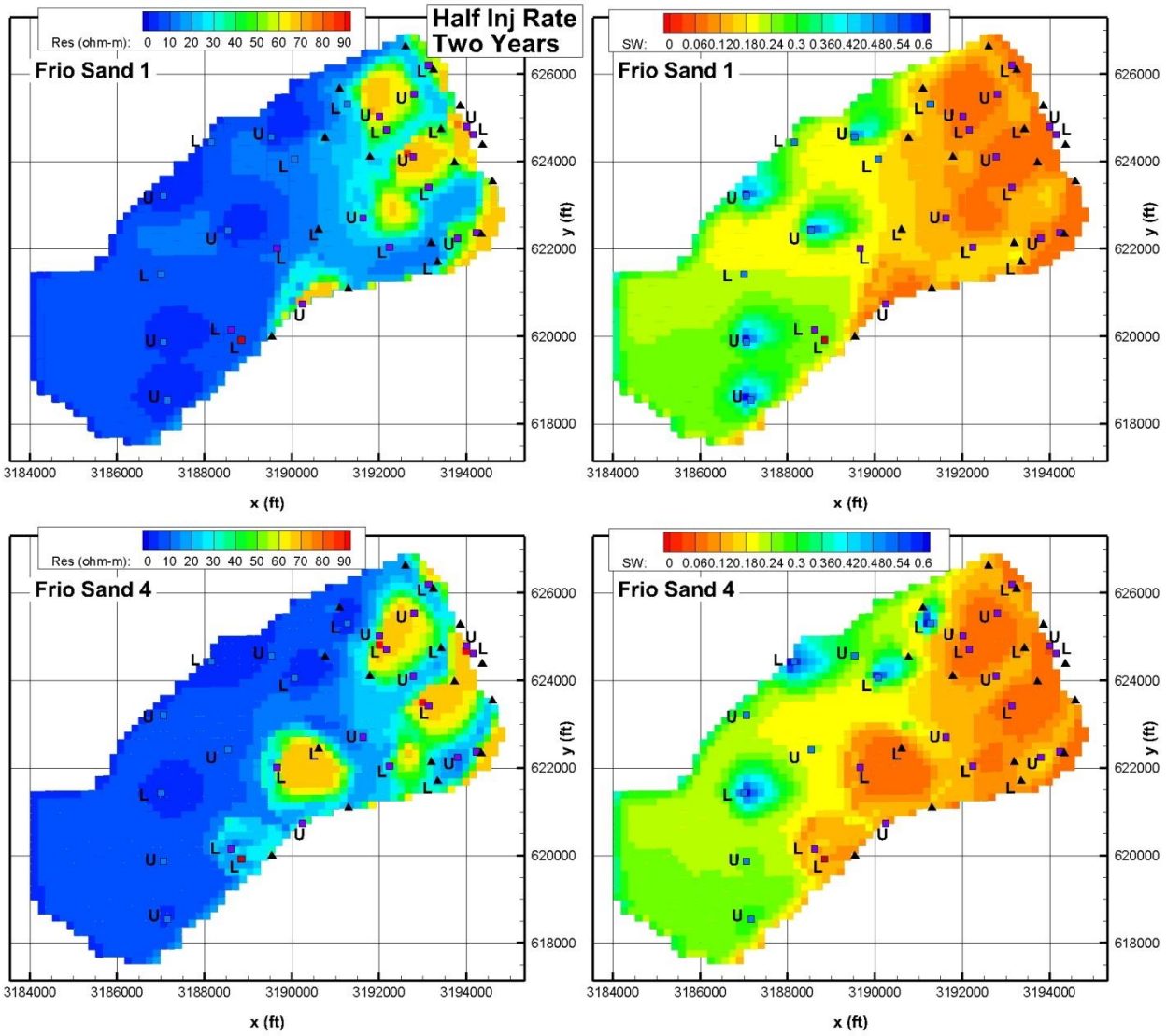


Figure 2.12. Model results for two years of $CO_2$ injection at half the injection rate, for the top model layer (Frio Sand 1) and the fourth model layer (Frio Sand 4). (Left) resistivity, (Right) aqueous phase saturation).

Generally, the model captures the key feature of the field data of showing a low-resistivity plume in the updip region of the model, which corresponds to lower aqueous phase saturation, and the distinct behavior for the upper and lower portions of the reservoir, corresponding to the U or L interval for the injection wells. However, the model shows more distinct responses corresponding to individual injection wells, with less spreading between wells, than the field data does. In particular, the updip migration of injected $CO_2$ is apparent around most WAG injectors.

As expected, comparing full- and half-injection-rate cases at 1 year shows bigger changes in the former. One might expect that the 1-year full-rate response (Figure 2.10) and the 2-year half-rate response (Figure 2.12) would be identical because the same total amount of $CO_2$ has been

injected, but there are subtle differences, including more spreading and greater updip migration visible in Figure 2.12.

One interesting feature noted in the model but missing from the field data is the resistivity decrease and aqueous phase saturation increase around the water injection wells in the down-dip portion of the reservoir. This suggests that the modeled quantity of water injected in these wells may be too large.

Figures 2.13 and 2.14 shows modeled gas, water, and oil flow rate as a function of time for the three production wells known to have an open interval in the lower half of the formation (wells circled in orange in Figure 2.7). One point of field data is available for comparison, but the time it corresponds to is not known. Figure 2.13 shows results for the full-injection-rate case, and Figure 2.14 shows results for the half-injection rate case, which generally match the field data better.

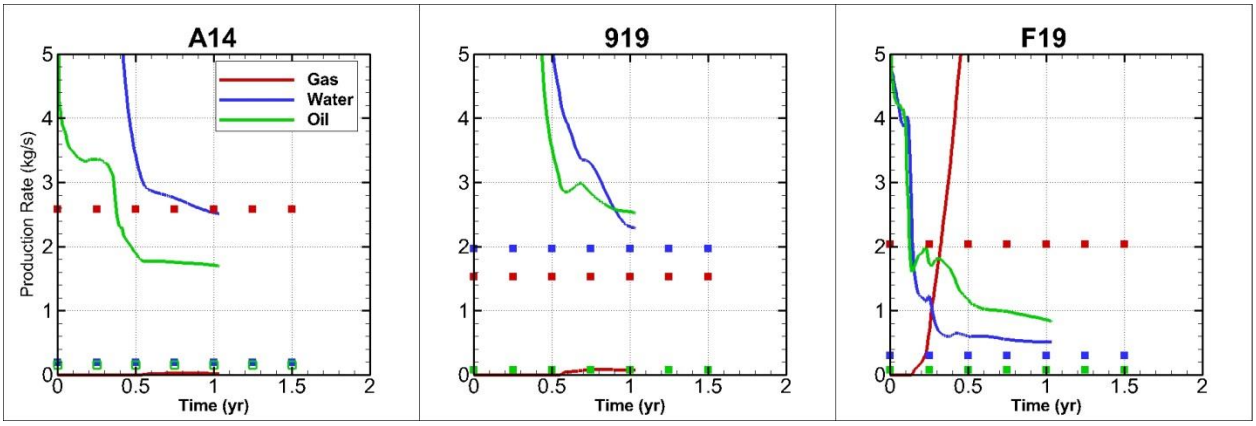


Figure 2.13. Modeled production rates from the lower level production wells at cells A14, 919, and F19 (lines) and one value of field data (dots – time unknown), for the full-injection-rate case.

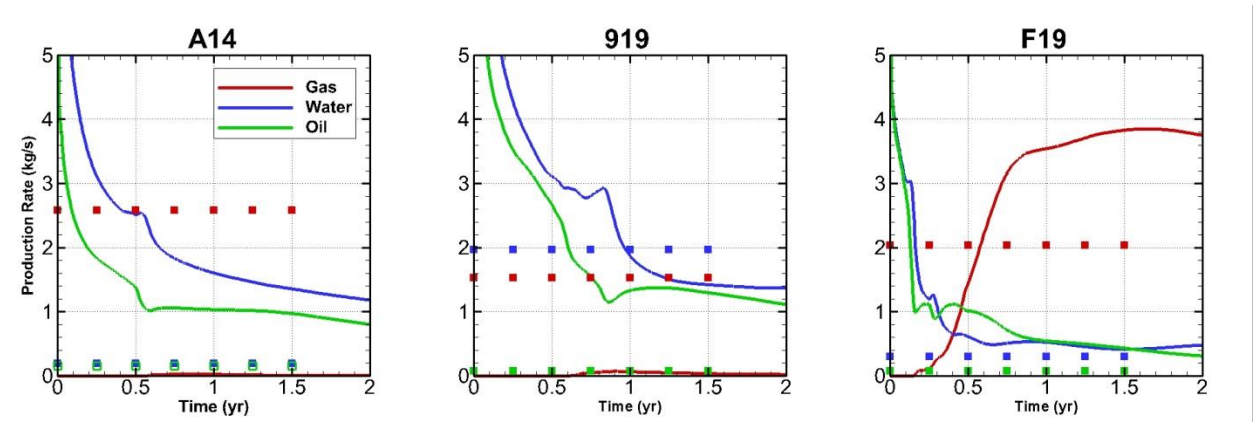


Figure 2.14. Modeled production rates from the lower level production wells at cells A14, 919, and F19 (lines) and one value of field data (dots – time unknown), for the half-injection-rate case.

The preceding model results are the only ones that can be compared to field data, but it is of interest to look at other results also, to get a better sense of what is occurring during $CO_2$ injection. Figures 2.15 and 2.16 show gas saturation and oil saturation distributions for the half-injection-rate case at 1 year and 2 years, respectively. There is a good correspondence between resistivity high (Figures 2.11 and 2.12) and gas saturation distribution, confirming that it is injected $CO_2$ that is the primary cause of the resistivity anomaly, rather than changes in oil saturation.

The oil saturation distributions show how $CO_2$-EOR is effective at pushing oil away from the injection wells toward the production wells. Note in particular in Figure 2.16, Frio Sand 4, how a ring of increased oil saturation forms around the injector near x = 3190000 ft, y = 622000 ft.

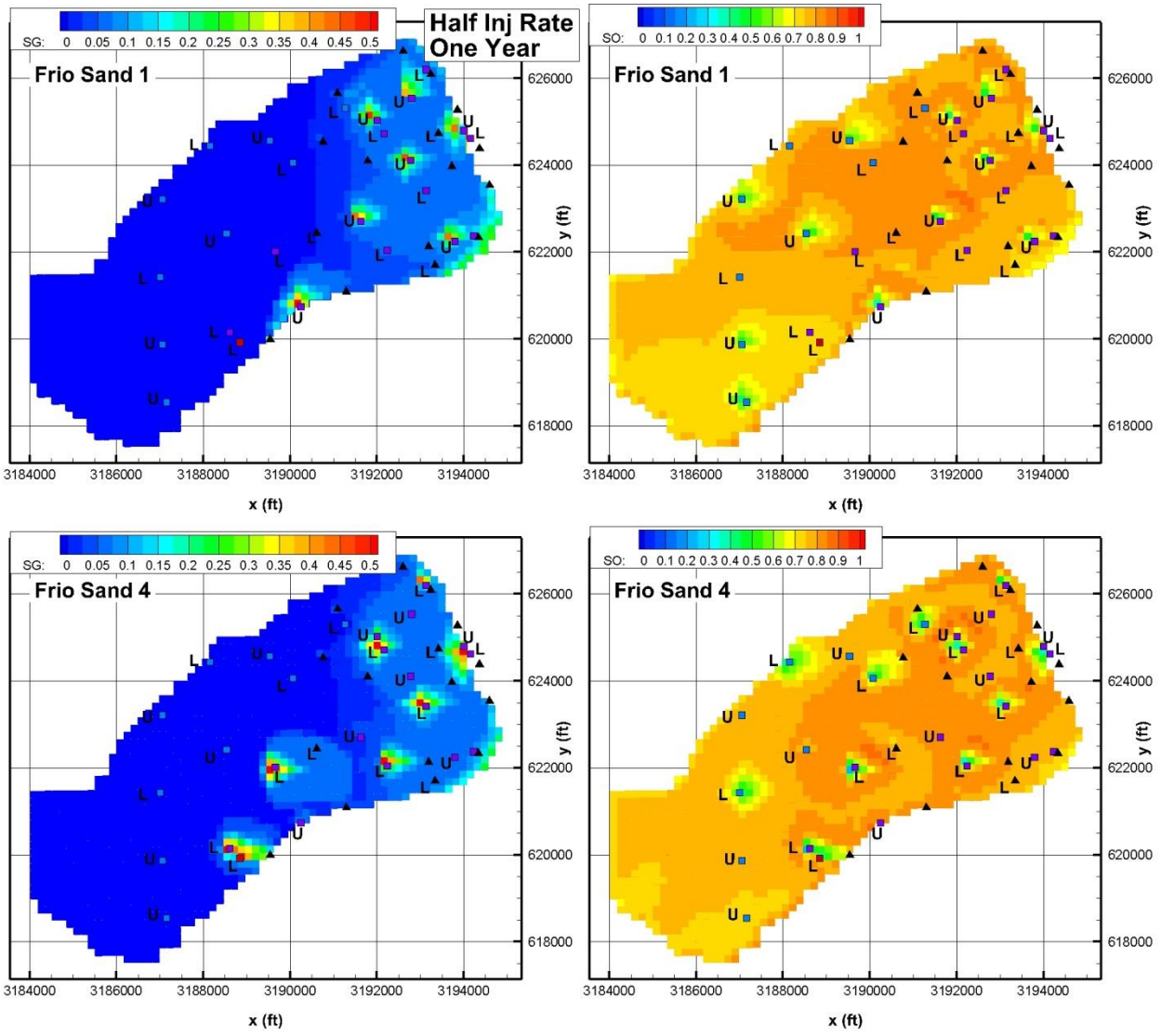


Figure 2.15. Model results (Left – gas saturation, Right – oil saturation) for one year of $CO_2$ injection at half the injection rate, for the top model layer (Frio Sand 1) and the fourth model layer (Frio Sand 4).

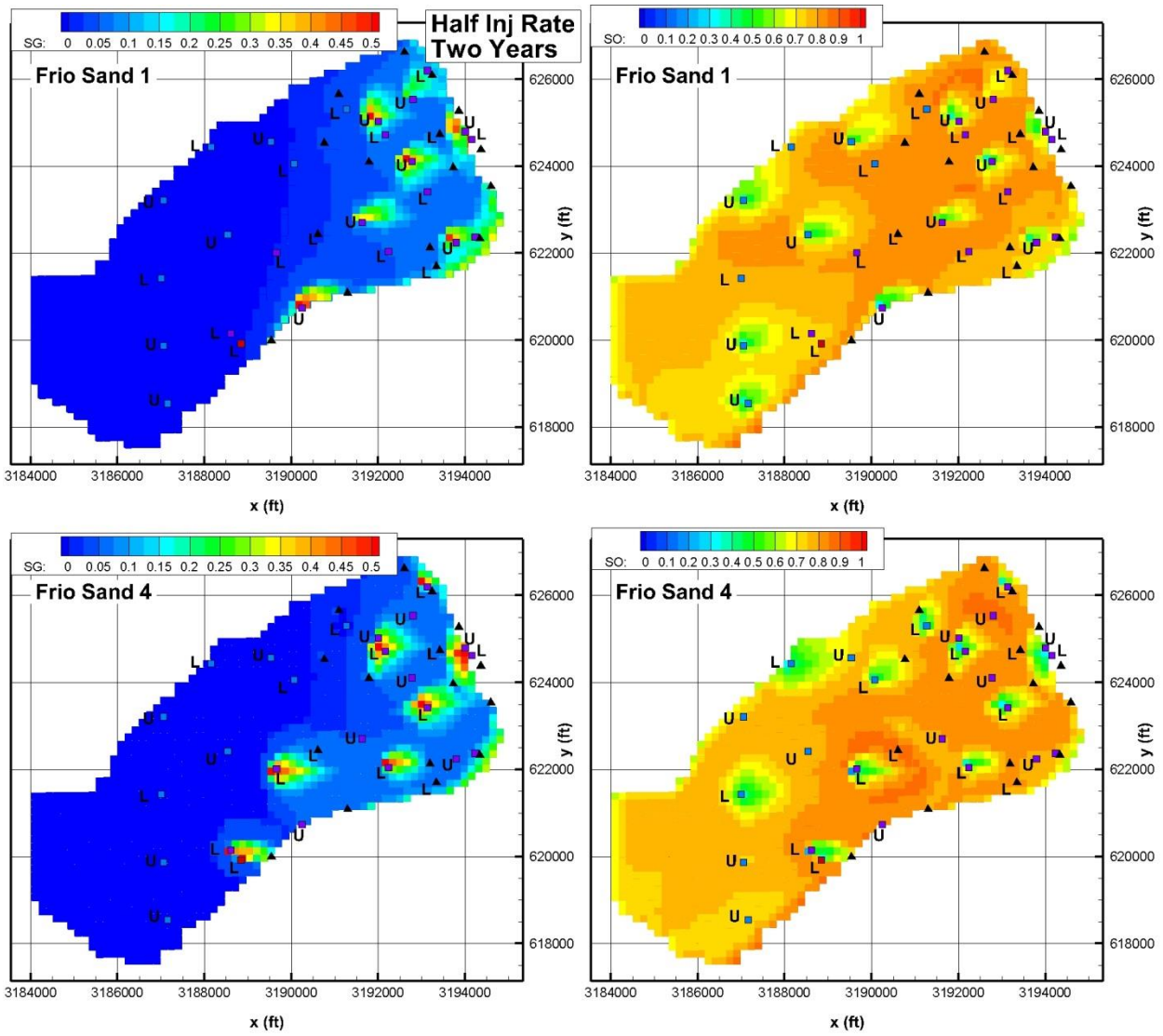


Figure 2.16. Model results (Left – gas saturation, Right – oil saturation) for two years of $CO_2$ injection at half the injection rate, for the top model layer (Frio Sand 1) and the fourth model layer (Frio Sand 4).

Figures 2.17 and 2.18 show how the gas saturation distributions (Figures 2.15 and 2.16), are partitioned between $CO_2$ and $CH_4$. The variables plotted are the product of gas saturation and mole fraction of $CO_2$ or $CH_4$. Recall that there is no gas phase at all in the reservoir at the onset of $CO_2$ injection. As gaseous $CO_2$ is injected, some of the $CH_4$ dissolved in the oil phase and aqueous phase exsolves. Note how the $CH_4$ tends to form a halo around the $CO_2$ emanating from the injection wells. The lighter $CH_4$ also moves buoyantly to the highest elevation in the reservoir, near x = 3194000 ft, y = 622000-623000 ft.

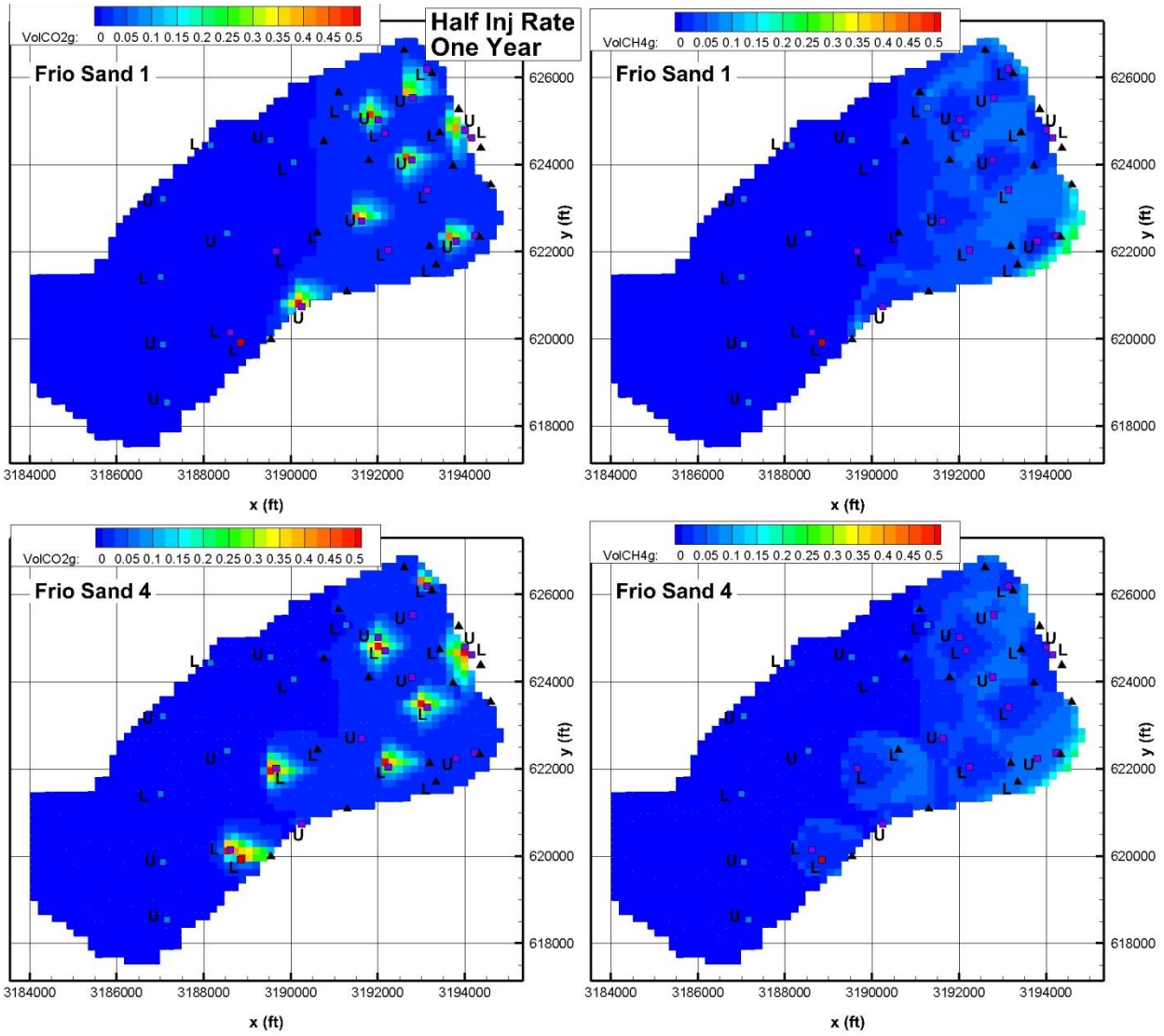


Figure 2.17. Model results (Left – volume of $CO_2$ in the gas phase, Right – volume of $CH_4$ in the gas phase) for one year of $CO_2$ injection at half the injection rate, for the top model layer (Frio Sand 1) and the fourth model layer (Frio Sand 4).

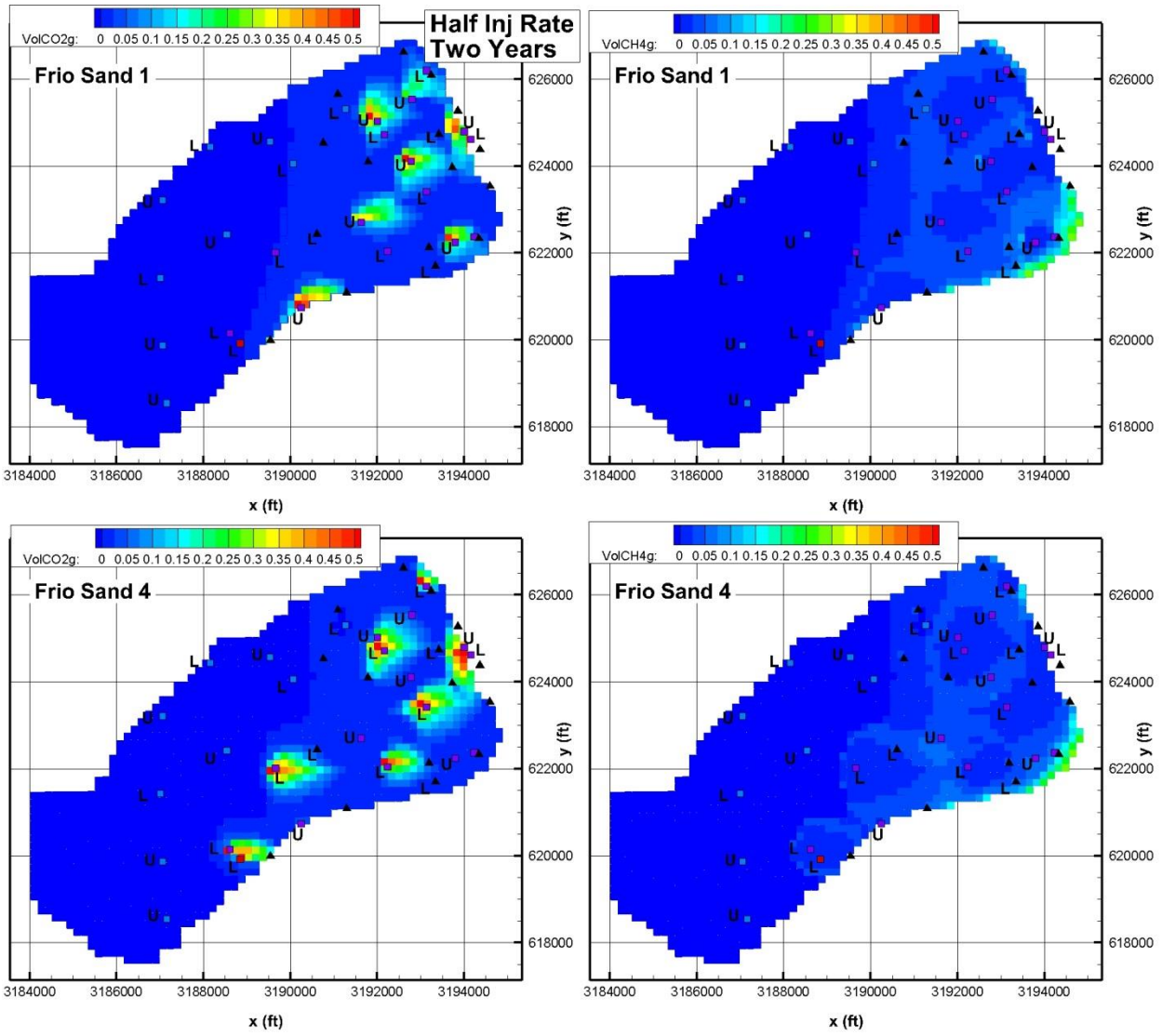


Figure 2.18. Model results (Left – volume of $CO_2$ in the gas phase, Right – volume of $CH_4$ in the gas phase) for two years of $CO_2$ injection at half the injection rate, for the top model layer (Frio Sand 1) and the fourth model layer (Frio Sand 4).

## 2.8 Conclusions and future work

The practical simplifications needed to simulate an actual operating oil field preclude using the present model to get an accurate history match or to make detailed predictions. Rather, the modeling is intended to illustrate the general trends occurring during $CO_2$-EOR in the BC fault block and to indicate where more detailed information is needed.

The multi-phase fluid flow occurring as a result of water and $CO_2$ injection accompanied by water, gas, and oil production that is simulated by the model is reasonable and compares moderately well with the field data available.

The present model could be improved in many ways to provide a better representation of flow and transport processes accompanying $CO_2$-EOR.

a. Represent wells and field operating conditions more accurately. Use actual upper/lower perforations for injection wells, and actual injection rates and schedules. Use a simplified wellbore model for injectors and a deliverability model for producers.
b. Finer vertical grid resolution. Currently the model has one layer per sand layer, but the second and third layers are much thicker than the other layers and would benefit by subdividing into two or three layers each, resulting in a total of 9 or 10 layers. More importantly, the actual depths and variable thicknesses of the layers can be incorporated into the model, rather than simply using tilted planes, as is done now, which will enable the movement of the $CO_2$ plume to be represented better.
c. Use a more detailed representation of heavy oil components.
d. Include intra-block faults and consider alternative lateral boundary conditions.

## Acknowledgements

Thanks to Kris MacLennan of GroundMetrics, Inc. for providing resistivity data, guidance, and a real-world perspective for the modeling studies, and to Curt Oldenburg of Lawrence Berkeley National Laboratory for his careful review of this report. This material is based upon work supported by the U.S. Department of Energy, Office of Science, under Award Number DE-SC0009709. This work was performed at Lawrence Berkeley National Laboratory of the US Department of Energy (DOE) under Contract No. DE-AC02-05CH11231.

## References

Pan, L., and C.M. Oldenburg, TOGA: A TOUGH code for modeling three-phase, multi-component, and non-isothermal processes involved in $CO_2$-based Enhanced Oil Recovery, *Rep. LBNL-1006472*, Lawrence Berkeley National Lab., Berkeley, CA, 2016.

Pruess, K., The TOUGH codes - a family of simulation tools for multiphase flow and transport processes in permeable media, *Vadose Zone J.*, 3(3), pp 738–746, 2004.